Manuals, Monographs and Data Series

Crevice Corrosion

Journal:	*ASTM-Books*
Manuscript ID	BOOKS-2019-0034.R1
Manuscript Type:	Manuals
Date Submitted by the Author:	n/a
Complete List of Authors:	Ianuzzi, Mariano; Curtin University, Curtin Corrosion Centre Hornus, Edgar; Curtin University, Curtin Corrosion Centre Salasi, Mobin; Curtin University, Curtin Corrosion Centre
ASTM Committees and Subcommittees:	G01.05 Laboratory Corrosion Tests < G01 Committee on Corrosion of Metals
Keywords:	crevice corrosion, stainless steels, nickel alloys, test methods

CREVICE CORROSION

Mariano Iannuzzi[1], Edgar Hornus[1], Mobin Salasi[1]

[1]Curtin Corrosion Centre, Curtin University, Perth, Australia,

INTRODUCTION

Crevice corrosion—defined in ASTM G193 as "the localized corrosion of a metal or alloy surface at, or immediately adjacent to, an area that is shielded from full exposure to the environment because of close proximity of the metal or alloy to the surface of another material or an adjacent surface of the same metal or alloy,"—affects most metals and alloys and is among the most damaging forms of corrosion.[1] Crevice geometries can be found on a wide range of structures and components, e.g., flanges, threaded connections, lap joints, as well as under deposits and damaged coatings.[2]

Metals and alloys that develop a passive film are prone to crevice corrosion. In contrast, those that do not form a surface film tend to corrode uniformly outside the occluded region due to the ready access to the oxidizing species that support the cathodic reactions.[3] Stainless steels, especially those with little to no molybdenum, some nickel-based alloys, and aluminum alloys are particularly susceptible to crevice corrosion.[4] Moreover, materials that have been shown highly resistant to pitting corrosion, such as titanium and Ti-based alloys, suffer crevice corrosion in specific environments. [5, 6]

As will be discussed below, there are many similarities between pitting and crevice corrosion mechanisms. Researchers have argued that for many material-environment combinations, the same mechanism is at play.[7] While some authors suggest that crevice corrosion is a particular form of pitting corrosion, all pits are crevices as “pits cannot be stable until a crevice-like cavity develops.”[8] It is important to emphasize that crevice corrosion resistance is not a property of a material. In this regard, the response of a particular alloy system to a given environment determines the crevice corrosion susceptibility. For example, iron and carbon steels do not suffer crevice corrosion in strong acids since they do not develop a passive film but become susceptible in alkaline environments free of aggressive species where a passive film is thermodynamically stable.[9]

Crevice Geometry

A crevice is formed when two surfaces, at least one being metallic, are in close proximity and immersed in an electrolyte that can promote crevice corrosion. Examples of materials that can cause crevice corrosion include metals, wood, plastics, ceramics, rubbers, glasses, concrete, asbestos, waxes, sand

deposits, marine growth, coatings, etc.[3, 10-12] FIG. 1 illustrates an idealized crevice. As seen in FIG. 1, the crevice geometry is described by the opening or gap (*g*) and the length (L), measured as the distance from the crevice mouth.[3] The gap has to be wide enough to allow the ingress of the solution, but sufficiently tight to promote the formation of an occluded environment within the cavity. Openings between 0.1 and 100 µm have been typically found to cause crevice corrosion.[2] Crevice corrosion rarely occurs in wide (e.g., >3mm) grooves or slots. The crevice is, thus, divided into two regions. The external surface that is freely exposed to the environment and the shielded or creviced area exposed to a stagnant solution.

The gap in a real crevice is not a fixed value. Indeed, at the microscale, the two mating surfaces have a series of ridges and asperities, as shown by the surface profiles in the call-out in FIG. 1. The surface profiles seen in FIG. 1 correspond to an ASTM A480 surface finish no. 1 [13] with a peak-to-peak distance of approximately 15 µm. As a result, a real crevice has a complex and distributed geometry that cannot be defined rigorously, resulting in "a wide range of crevice gaps, including areas of direct, intimate contact."[2]

Objectives

Today, there is a large number of accepted tests to study crevice corrosion phenomena. The different methodologies can be used for comparing and ranking alloys, quality control, assessing the effects of changes in manufacturing routes and alloy composition on crevice corrosion resistance, as well as in evaluations to determine critical temperatures and potentials and induction times.

The goal of the chapter is to describe the various standard test methods available to the corrosion specialist as well as adaptations to study specific crevice corrosion parameters and prevention strategies, e.g., the use of inhibitors. The focus is on test methods developed by the ASTM Committee G-1 on corrosion of metals, but other procedures are also included. While the test principles have been applied to many alloy systems, the scope of the chapter is on stainless steels and nickel-based alloys.

CREVICE CORROSION MECHANISMS

Differential aeration and chloride concentration

It was realized early on that the metals and alloys that were easily passivated were also those that appeared more susceptible to crevice corrosion. [14] Mears and Evans [10] and Uhlig [15] were the first to propose that oxygen depletion within the crevice was the main driving force leading to the

destabilization of the passive film inside the cavity. However, a mechanism solely based on concentration cells failed to explain many experimental observations.[16]

In the 1950s, Rosenfeld and Marshakov [17] pioneered crevice corrosion experimental methods. The authors suggested that crevice corrosion occurred through a combination of (i) depletion in oxygen (or a corrosion inhibitor) in the crevice, (ii) local acidification, and (iii) shift in the potential to more negative values, where active dissolution would take place. Many of the modern crevice corrosion principles are based on the findings by Rosenfeld and Marshakov.

It is now well established that the mechanisms that drive a growing crevice are identical to those promoting a growing pit.[8] In this regard, when a passive metal or alloy, e.g., an austenitic stainless steel such as UNS S30400, partially covered by a non-metallic surface is exposed to aerated seawater (pH = 8.0), the electrochemical reactions are the dissolution of the metal and the reduction of dissolved oxygen, Eq. 1 and Eq. 2.[3]

$$\mathrm{Me} \rightarrow \mathrm{Me}^{z+} + ze^{-} \quad \text{(Eq. 1)}$$

$$\mathrm{O_2} + 2\mathrm{H_2O} + 4\mathrm{e}^{-} \rightarrow 4\mathrm{OH}^{-} \quad \text{(Eq. 2)}$$

Initially, these reactions occur inside and outside the crevice. After a given time, oxygen is depleted inside the cavity due to restrictions imposed by convection within the occluded surface. The dissolution of the metal continues within the crevice, resulting in excess of metal cations (e.g., Fe^{2+}, Cr^{3+}, Al^{3+}, etc). As the corrosion process continues, the concentrated metal cations within the stagnant cavity hydrolyze according to Eq 3, which results in the formation of H^{+}.[18-20] The excess of metal cations is necessarily balanced by the migration of anions such as chloride ions (Cl^{-}) from the bulk into the cavity, which ensures charge neutrality. As a result, the concentration of metal chlorides increases inside the crevice.

$$Me^{z+} + \mathrm{H_2O} \rightarrow \mathrm{Me}OH^{(z-1)+} + \mathrm{H}^{+} \quad \text{(Eq. 3)}$$

The formation of a local acidic environment increases the metal dissolution rate in the crevice, producing more protons, and increasing the Cl^{-} concentration further. This process is often referred to as autocatalytic. Concurrently, the oxygen reduction reaction accelerates on the outer surface to counteract the increased metal dissolution rate within the cavity, cathodically protecting the external surface. [3] Active metal dissolution occurs when the crevice solution concurrently has a sufficiently (i) low pH and a (ii) high concentration of Cl^{-}.[21] The pH at which the passive-to-active transition takes place is referred to as depassivation pH (pHd).[21] Oldfield named the solution that leads to the

depassivation of the alloy within the crevice gap "critical crevice solution" (CCS). [22] The formation of the CCS represents the transition from the initiation to the propagation stage. Although this model phenomenologically explained most experimental observations, it failed to rationalize the existence of a critical potential, above which crevice corrosion develops.[9] In this regard, the primary limitation of the Oldfield and Sutton's model is that it considered that the dissolution of cations (and their consequent hydrolysis) was proportional to the passive current density, i_{pass}. Since i_{pass} is constant over a broad potential range, the model is unable to account for the existence of critical potentials, both initiation and repassivation potentials. Moreover, Oldfield and Sutton's description cannot take into consideration the effect of inhibitive species such as, e.g., fluorides, which increase the passive current density of UNS Alloy 22 (UNS N06022) in hot chloride environments. [23]

The critical acidification model

Galvele [18] and later Oldfield and Sutton [21, 24] were the first to consider the transport of species in and out of pits and crevices. These models have since then been improved and expanded to provide, in some instances, not just conceptual observations but also numerical solutions.[20, 25, 26] Galvele proposed that since crevice corrosion is believed to be due to localized acidification, crevice corrosion could be described by the critical "x·i" parameter (referred to as pitting or crevice stability product) used in his mathematical framework.[9] In the pitting or crevice stability product, *x* represents the diffusion path and *i* the current density of a pit or crevice, FIG. 3. [18] Localized corrosion propagates stably above a critical *x·i* value, which is constant for a given material in a specific electrolyte. According to Galvele and later Newman,[8] pitting and crevice corrosion are similar from an electrochemical point of view; the only difference being the geometric characteristics of the sample, i.e., a different diffusion path. Accordingly, the critical potential for stable crevice propagation (E_{Crit}) can be described as:

$$E_{\mathrm{Crit}} = E^{*}_{\mathrm{Corr}} + \eta + \Phi + E_{\mathrm{inh}} \qquad \text{(Eq. 4)}$$

In Eq. 4, E^{*}_{Corr} is the corrosion potential in a simulated crevice electrolyte, η the polarization needed to reach the critical x·i value, Φ the electrical potential induced by the migration of the aggressive anions to the crevice (or the bottom of a pit), and E_{inh} the contribution of the presence of inhibitors in the solution [16]. However, E_{inh} cannot always be experimentally separated from other factors. [27, 28] The validity of Eq. 4 has been first confirmed by Newman et al. [29] and studied in numerous investigations.[27, 30-35] The different parameters in Eq. 4 can be measured experimentally by conducting anodic polarization experiments in crevice-like solutions.[32-34, 36] The effects of alloying elements on the crevice

corrosion resistance are reflected in changes in E^{*}_{Corr} and η.[34, 35] Eq. 4 also explains why certain metals and alloys are susceptible to crevice corrosion but not to pitting. Indeed, η can be used as a measure of the crevice corrosion resistance of an alloy. [30-34] In this regard, the larger the value of η, the broader the range of potentials where crevice corrosion would be exclusively observed. For stainless steels and nickel alloys, the values of η range from +470 to +1000 mV, which explains why crevice corrosion occurs much more readily than pitting.[34]

As discussed by Galvele, Wood et al. provided a clear experimental demonstration of the correlation between pitting and crevice corrosion.[37] In their pioneer work, the authors conducted potentiostatic experiments on freely exposed and creviced UNS S30400 stainless steel samples. The crevice was formed using glass microscope covers, leading to *g* values between 50 and 150 µm. The samples were exposed to 5 wt.% NaCl (pH = 8.0) at room temperature. Wood et al. found that at +600 $mV_{SCE,}$ pitting corrosion initiated not only on the outer surface but also inside the crevice. In contrast, when new samples were polarized at +400 mV_{SCE}, the attack occurred exclusively inside the crevice. Crevice corrosion started as individual pits that spread laterally as the attack progressed, leading the authors to the idea that crevice corrosion is “lateral pitting” within the crevice gap.

Today, it is accepted that the accelerated attack within the crevice can manifest as uniform dissolution, pitting, or both. [24] FIG. 2 illustrates three common forms of corrosion attack occurring inside a crevice on different stainless steels. Stockert and Boehni [38], and later, Laycock et al.[8] suggested that pit nucleation within crevices occurs even at small applied potentials, resulting in measurable current noise. The current and, hence, the dissolution rate increase sharply above the $E_{Crit,}$ and stable pit propagation takes place and leads to the formation of metal-chloride salts.

Ohmic potential drop

The passage of current from the external surface to the crevice through a solution of finite conductivity results in an ohmic potential drop and, thus, the potential inside the crevice will be lower (i.e., more negative) than at the surface. In systems that exhibit an active-passive behavior in the bulk electrolyte, the ohmic potential drop in the crevice can stabilize pit growth by decreasing the local potential into the active range.[39] However, this mechanism, proposed by Pickering, does not apply to a system where an active-to-passive transition does not occur. Indeed, in systems that show spontaneous passive behavior, a decrease in potential has a negative effect on crevice corrosion stability.

Stages of crevice corrosion

The crevice corrosion process can be, then, summarized in four stages, namely, (i) oxygen consumption within the crevice, (ii) increase in H^+ and Cl^- in the crevice, (iii) stabilization of a critical H^+ concentration above a threshold x·i value, and (iv) propagation. While the first stage is key for carbon and low alloy steels in alkaline solutions, which suffer corrosion by differential concentration cells [40], it is of less importance for passive alloys. Conversely, the second stage is crucial to explain the depassivation of passive alloys. In this regard, the migration of chlorides supports the reduction in pH resulting in an acidic solution of lower pH than predicted only by cation hydrolysis, since a high concentration of chlorides results in a higher activity coefficient for protons (H^+). [41, 42]

Given the similarities between pitting and crevice corrosion discussed above, it is reasonable to conceptually adapt the Li-Scully-Frankel (LSF) framework to describe crevice corrosion.[43-46] Thus, the state of a crevice can be fully described in terms of a critical potential (E_{Crit}), a critical temperature (T_{Crit}), and an induction time. The existence of E_{Crit} was discussed above. Temperature has a strong influence on localized corrosion phenomena.[47] Experimentally, pitting and crevice corrosion are observed only above specific temperatures (referred to as critical pitting or crevice temperature, CCP and CCT, respectively) that are usually defined within a narrow 1-2 °C range. [48-50] The length of time required to develop a critical crevice solution with a particular crevice geometry, i.e., a given "x" in the *x·i* stability product, is referred to as induction time. In this regard, the induction time can be seen as a measure of the effective crevice corrosion resistance of an alloy. Crevice corrosion occurs at lower temperatures and in less time (a shorter induction period) than pitting corrosion.[47, 51]

A detailed discussion of the different crevice corrosion mechanisms is outside the scope of this chapter. More information on localized corrosion models and mechanisms can be found in the excellent reviews by Betts and Boulton, Pickering, Frankel, Newman, and a recent Faraday Discussions on Localized Corrosion.[3, 52-55].

TEST METHODS TO ASSESS CREVICE CORROSION RESISTANCE

Different classification schemes could be used to group crevice corrosion test methods. Herein, the tests are primarily divided into two groups: (i) immersion or non-electrochemical and (ii) electrochemical testing. Electrochemical methods are, in turn, further classified as tests with and without external polarization. Likewise, methods that use an external polarization are subdivided into potentiostatic and potentiokinetic. Table 1 to Table 4 summarize the most common standard and custom crevice corrosion

techniques. The tables were organized based on the categories described above. Tables 1 to 4 illustrate the uses, exposure conditions, the type of crevice assembly, the duration, the procedure, and the recommended assessment, among other experimental considerations. For more details, the reader is advised to consider some of the excellent works cited in this chapter. [21, 22, 24, 56-59]

The Crevice Former

Before describing the various crevice corrosion test methods, it is necessary to discuss the use of crevice formers, in particular, the multiple-crevice assembly (MCA) as a means to rank and evaluate crevice corrosion resistance. Described by Anderson in the late 1970s, MCAs were first introduced to study crevice corrosion of stainless steels in seawater.[60] Today, MCAs are used not only on stainless steels, but also nickel, titanium, and aluminum alloys in virtually any process environment.[58, 61, 62]

An MCA is composed of several grooves and plateaus—typically between 12 and 20 slots—with a depth of approximately 0.5 mm. The purpose of the serrations is to create several crevice initiation sites within a single specimen, which should allow for statistical analysis with a few replicate tests. [58] MCAs are commonly made of polytetrafluoroethylene (PTFE), polychlorotrifluoroethylene (PCTFE), polyvinylidene difluoride (PVDF), ceramic, and PTFE tape-covered ceramic. The contact area of each crevice contact and the total contact area are important variables that need to be reported. FIG. 4a illustrates the various parts of a typical MCA that complies with ASTM G48. [63] In FIG. 4a, the bolts and nuts are made of highly corrosion-resistant materials, typically Titanium Grade 2 (UNS R50400) or a nickel-based alloy such as UNS N10276 or UNS N06022. The bolts and nuts are electrically insulated from the test specimen using, e.g., PTFE tape or a polymer insert.[64]

It has long been recognized that the tightness of a crevice former has a profound effect on the crevice corrosion severity, which in the laboratory is usually controlled by the applied torque. Akashi et al. studied, among other variables, the effect of torque on the crevice repassivation potential ($E_{R,\ Crev}$).[65] The authors found that if the torque was "too low" (i.e., below 0.98N·m) $E_{R,Crev}$ moved towards higher potentials, indicating a less severe crevice. However, for torque values between 0.98 and 3.9 N·m, $E_{R,Crev}$ became stable and reproducible. Presently, the ASTM G48 standard recommends a torque of 0.28 and 1.54 N·m for nickel-alloys and stainless steels, respectively. However, researchers have used torque values from 0.28 to 9.5 N·m with varying degrees of success. [33, 66]

Shan and co-workers investigated the effect of the crevice former material, i.e., polymer versus ceramic, as well as the influence of the surface finish of the MCA.[66] The authors used potentiokinetic and

potentiostatic test methods and evaluated PTFE, PCTFE, ceramic, and PTFE tape-covered ceramic crevice formers on UNS N06022 (Alloy C22). Results showed that PTFE tape-covered MCAs produced systematic and reproducible crevice corrosion of Alloy C22 in all tests. In contrast, as-fabricated ceramic crevice formers were not sufficiently severe. The severity increased as the MCA was polished to 1200 US-grit before assembly. Polymeric PTFE and PCTFE MCA were also less severe than the PTFE tape-covered formers, possibly due to the relaxation of the polymers by creep at the elevated temperature range of the tests. FIG. 4b illustrates a typical PTFE tape-covered MCA on an Alloy C22 sample.

In Europe, research was undertaken as part of the CREVCORR project—funded by the European Community between the years 2000 and 2003 under the "Competitive and Sustainable Growth" Programme—to develop a crevice corrosion qualification test for stainless steels used in marine environments.[67] The outcome of the CREVCORR project is presented in detail in the European Federation of Corrosion (EFC) Publication No 60 “Methodology of crevice corrosion testing for stainless steels in natural and treated seawaters.”[68] Regarding the type of crevice former, the CREVCORR project concluded that a spring-loaded crevice assembly, referred to as disc spring multiple crevice assembly (DSMCA), was the most suitable artificial crevice former.[69] The DSMCA uses a flat PVDC crevice former and employs disc springs to maintain a constant force instead of constant torque during testing, which is especially critical in long-term immersion tests at elevated temperatures.[70] FIG. 4c details the CREVCORR crevice configuration. The CREVCORR project also adapted the DSMCA configuration to evaluate stainless steel pipes. Finite-element modeling (FEM) was employed to quantify the clamping force distribution and the uniformity of the crevice condition within the crevice former. [71]

Shoesmith and coworkers developed a single crevice array to study crevice corrosion of highly resistant alloys such as titanium grade-2 [72] and Alloy 22 (UNS N06022) at high pressure, high temperature, or both [73]. The crevice electrode consists of a PTFE crevice former of a known area centered and pressed between two flat coupons; one cut from a plate of the metal or alloy of interest and the other cut from a thick polysulfone plate. The crevice assembly is formed by tightening the plates using corrosion-resistant bolts and nuts. The tightness is adjusted with the help of a PFTE "feeler," as described by the authors, using open-faced wrenches. [72] The approach was used by Shoesmith et al. to construct corrosion damage functions [74] as well as to determine the influence of temperature on crevice corrosion susceptibility.[72]. Many other non-standard methods have been used by researchers to create artificial

crevices for different purposes. For a more in-depth explanation, the reader could consult the work by Oldfield [22] and Kain [62].

NON-ELECTROCHEMICAL TEST METHODS

Non-electrochemical immersion tests involve immersing a creviced specimen for different lengths of time in solutions that often contain anions that promote crevice corrosion such as chlorides and, in some instances, an oxidizing agent that facilitates the initiation of crevice corrosion (e.g., Fe^{3+} cations). The crevice corrosion resistance is, then, determined based on mass loss and visual observations. Visual characterizations include crevice depth, number of crevice sites, location of the crevice attack within the cavity, and the corrosion morphology.

ASTM G48 is the most commonly used standard to assess pitting and crevice corrosion resistance of stainless steels and nickel-based alloys and to provide a quantitative ranking of crevice corrosion resistance. There are six test methods in the present version of the ASTM G48 standard (2011, re-approved in 2015). While Methods A, C, and E cover pitting corrosion resistance, Methods B, D, and F describe different techniques to assess crevice corrosion susceptibility. Additionally, ASTM G78 details guidelines to evaluate the crevice corrosion resistance of iron- and nickel-based alloys in seawater and other chloride environments.

Although ASTM G48 Methods B, D, and F and ASTM G78 are discussed in detail below, the reader should consult the latest version of the standards for a comprehensive description.

ASTM G48 Method B – The Rubber Band Test

The ASTM G48 Method B is used to assess the pitting and crevice corrosion resistance of stainless steels and nickel-based alloys to chloride-containing environments. The procedure involves immersing a creviced specimen in a 6 wt% $FeCl_3$ (equivalent to 10 wt% $FeCl_3 \cdot 6H_2O$) solution (unadjusted pH = 1.0 to 2.0) [75], designed to produce localized corrosion of UNS S30400 (type 304) stainless steel at room temperature. The relative performance of alloys in 6 wt% $FeCl_3$ correlated well with their performance in natural seawater at ambient temperature [76] and strongly oxidizing, low pH, chloride-containing environments [22]; however, exceptions have also been reported. [11, 22, 77, 78]

The standard recommends 22 ± 2 and 50 ± 2°C for the evaluation, but other values could be used depending on the expected corrosion resistance of the alloy. The artificial crevice is formed using two TFE-fluorocarbon blocks, 12.7 mm in diameter and 12.7 mm in height, secured by fluorinated O-rings or

rubber bands that should be low in sulfur (i.e., < 0.02%). The surface roughness of the crevice formers is not specified. A 25 by 55 mm test specimen is recommended as standard size, but other dimensions are allowed. According to the standard, both the surface finish and the thickness of the coupons can influence the results. The standard also recommends storing the samples in air for 24-h after grinding or pickling and before testing to restore the naturally occurring passive film. FIG. 5a illustrates a typical test specimen before exposure.

After assembling the crevice formers, the coupons are immersed in the electrolyte for 72-h, but other exposure times are also permitted. The standard, likewise, allows for sample removal and inspection; nevertheless, care should be exercised since sample withdrawals could lead to variations in the rate of attack. After the predetermined exposure duration, the samples are removed from the solution, visually inspected, and weighted with a minimum accuracy of 0.001 g. ASTM G46 can be used as a guide for characterizing the extent of the attack.

The rubber-band method is inexpensive, easy, fast to assemble, and produces useful comparative results in a short time. However, the ASTM G48 Method B technique has a few disadvantages and limitations. For example, as seen in FIG. 5b, in certain alloys, particularly the less alloyed materials such as type 304 stainless steel, crevice can initiate at the contact point between the rubber bands and the specimen. Indeed, similar approaches were used in classical corrosion lectures to demonstrate that stainless steels could be “cut in half” with a rubber band. [16] Likewise, the test is invalid if either rubber band or O-ring breaks during testing, and the compressive pressure exerted by the rubber band onto the crevice formers is not uniform and can be difficult to replicate. Moreover, DeForce has recently shown that the type of rubber band used affects the results. [79] According to the authors, "specifying the rubber band elasticity (or rubber content) can improve the repeatability of ASTM G48 Method B." Lastly, while the mass loss is recorded after testing, there is currently no acceptance criterion. Producers and end-users have commercially accepted criteria such as a maximum of 0.038 mm crevice depth and 0.2 mg/cm^2 mass loss. In all cases, the pass or fail criteria shall be agreed between the user and the vendor.

ASTM G48 Methods D and F — Crevice Corrosion Temperature

Methods D (nickel- and chromium-bearing alloys) and F (stainless steels) overcome some of the limitations of the rubber band technique and allow the determination of the critical crevice temperature (CCT) of a material. In the standard, the CCT is defined as the minimum temperature, in °C, to produce crevice attack at least 0.025-mm deep on the bold surface of a specimen beneath the crevice former,

ignoring edge attack. The methods can also be used to rank alloy performance, aid in materials selection, and the design of new materials.[56, 80-83]

Methods D and F involve immersing creviced samples in acidified 6 wt% $FeCl_3$ + 1 wt% HCl (pH adjusted to pH = 1.0) for a period of time. Both methods use TFE-fluorocarbon MCA, and various geometries and construction materials are allowed. Method D recommends a torque of 0.28 N·m, whereas Method F suggests 1.58 N·m for stainless steel. However, authors have reported that applied torque values between 2 and 8 N·m were required to produce the most reproducible crevice corrosion results when evaluating highly corrosion-resistant nickel alloys. [84] The recommended duration of the immersion is 72-h (Method D) and 24-h (Method F). The length of the tests was evaluated by interlaboratory testing.

The initial temperature of the test solution may be estimated using the empirical expressions shown in Eq. 5 and 6. The minimum temperature is 0 °C and the maximum 85 °C due to the thermal degradation of the ferric chloride electrolyte.

$$\text{Method D: } (1.5 \times \%\text{Cr}) + (1.9 \times \text{Mo}) + (4.9 \times \%\text{Nb}) + (8.6 \times \%\text{W}) - 36.2 \qquad \text{Eq. 5}$$

$$\text{Method F: } (3.2 \times \%\text{Cr}) + (7.5 \times \text{Mo}) + (10.5 \times \%\text{N}) + (8.6 \times \%\text{W}) - 81.0 \qquad \text{Eq. 6}$$

A chief limitation of Eq. 5 and 6 is that the empirical expressions consider the effects of bulk composition alone, without taking into account the influence of alloy microstructure. For example, sensitized and properly annealed stainless steels will have identical CCT values according to Eq 5, yet the actual CCT will be drastically lower in the sensitized samples given the local depletion of chromium and molybdenum adjacent to, e.g., chromium carbides.[85, 86] Likewise, the expressions fail to capture the complex and intricate effects of alloying elements. Moreover, the equations were obtained by regression analysis using a limited set of alloys.[86] Interestingly, alloy C-276, which has a nominal composition of 15.5 wt% Cr, 16 wt% Mo, and 4 wt% W, would have a predicted CCT = 51.85 °C, whereas the more corrosion resistant alloy C22 (22 wt% Cr, 13% Mo, and 3wt%W) should have a CCT of approximately 47°C.

Testing shall begin at the nearest increment of 5 °C, estimated based on Eq. 5 or Eq. 6. The temperature shall be recorded and maintained within ±1 °C during testing. Only one specimen is permitted per test vessel. The samples are removed at the end of the exposure, rinsed with deionized water, and scrubbed with a nylon brush under running water to remove loosely adhered corrosion products, and dried using compressed air or nitrogen gas.

The specimens are then visually inspected after cleaning, and the weight loss measured with a precision of 0.001g. The recommendations of ASTM G46 can be followed to quantify the crevice attack. During the visual examination, the location of the crevice attack shall be determined, as well as the number of MCA sites showing signs of crevice corrosion. A full characterization includes the determination of the greatest depth of attack. As per ASTM G48, crevice corrosion is considered to be present if the local attack is 25 µm or higher in-depth, but no weight-loss acceptance criterion is given in the standard.

The CCT obtained by the ASTM G48 standard must be interpreted with caution. Although CCT values are well defined within a narrow range of temperatures, the CCT is not a property of a material, but a function of the experimental methodology. The test technique, the composition of the environment, the resulting corrosion potential in the solution, and the presence of inhibiting species all influence CCT results. Indeed, high chloride concentrations, and corrosion potentials, and long exposure times tend to result in lower CCT. [87]

Researchers have shown that the critical pitting temperature (CPT) and the CCT follow a similar trend with alloy composition,[87] which has been traditionally captured in the Pitting Resistant Equivalent (PRE) expression. Different expressions have been proposed to define the PRE of stainless steels and nickel alloys, and a detailed discussion is outside the scope of the current chapter. For more information, the work of Lorentz and Medawar [88], Malik et al. [87], and Jargelius-Pettersson [89] can be consulted. Presently, various international standards such as NORSOK M-001[90] and ISO 21457[91], respectively, define PRE as:

$$\mathrm{PRE} = \%\mathrm{Cr} + 3.3 \times \%\mathrm{Mo} + 16 \times \mathrm{N} \qquad \text{Eq. 7}$$

$$\mathrm{PRE} = \%\mathrm{Cr} + 3.3 \times (\%\mathrm{Mo} + 0.5 \times \mathrm{W}) + 16 \times \mathrm{N} \qquad \text{Eq. 8}$$

In Eq. 7 and 8, the concentrations are in weight percent. Qualitatively, the higher the PRE, the better the localized corrosion resistance of an alloy. Garner showed that both the CPT and the CCT of various stainless steels and nickel alloys correlated well with their respective PRE, i.e., CCT increased with the degree of alloying, especially their molybdenum content.[76] CCT values were also lower than CPT. In this regard, the difference between CCT and CPT was about 20 °C for the low PRE alloys (i.e., PRE = 24) and increased to approximately 50 °C for UNS S31254, which has a PRE of about 43. A conclusion that can be drawn from Garner's work is that the more highly alloyed corrosion resistant alloys (CRAs) can be susceptible to crevice corrosion while maintaining an excellent pitting corrosion resistance as discussed previously in this chapter. Recently, Klapper et al. produced a comprehensive compilation of CPT and

CCT values for a broad range of nickel alloys with PRE values ranging from 25 to approximately 70.[92] Klapper et al. results agree well with the work by Garner, with CCT values for alloys with a PRE of 25 being 40 °C lower than CPT. The difference between CPT and CCT increased to more than 80 °C for alloys with a PRE between 68 and 70. Likewise, the crevice corrosion induction time is typically shorter than that of pitting corrosion.[24, 93] Consequently, the duration of pitting tests is longer than a crevice test in the same environment. Lastly, CPT values are more reproducible than CCT (i.e., 2.5 vs. 10 °C).[47, 70, 94]

Precision and bias in critical temperature tests

As detailed in ASTM G48, the precision of Methods D and F for measuring the pitting and crevice corrosion resistance was determined in an interlaboratory test program where seven laboratories carried out triplicate tests on four materials. The results of these tests are given in Table 5. Results were consistent among laboratories, and there were no statistically significant variations between the materials in either repeatability or reproducibility. [95]

ASTM G78 — Crevice corrosion susceptibility in seawater

ASTM G78 is used to determine crevice corrosion susceptibility in seawater and other chloride environments. The scope of the standard is on iron- and nickel-based alloys, but it can be applied to other alloy systems. The standard suggests a multitude of different crevice former geometries, including MCA of various designs, O-rings, gaskets, strips, and coatings if testing complex geometries. Specimens could be flat, cylindrical, or have intricate shapes and be made of different polymers—including transparent acrylics—ceramics, glass, metals, wood, rubbers, etc. Specimens shall maintain a constant bodily exposed to shielded area ratio to ensure reproducible results that are not restricted by the cathode area.

The exposure temperature is user-defined, and it shall be maintained within 2 °C and recorded during testing. As with ASTM G48, tests at different temperatures can be used to determine the CCT. The recommended immersion time is 30 days. Sampling at different time intervals is permitted. A test program can be designed to quantify the crevice induction time by carefully planning frequent extraction intervals.

After immersion, the specimens are visually inspected to determine the maximum crevice depth—measured to the nearest 0.01 mm—and the affected area. When using MCA, the number of segments

showing crevice corrosion should also be reported. In addition, samples shall be weighted after exposure to determine weight loss.

Natural versus synthetic seawater

It is common to use either a 3.5 wt% NaCl solution or the ASTM D1141 [96] artificial seawater composition to simulate natural seawater in the laboratory. While these methods reproduce the chemical concentration of natural seawater, they do not take into account the influence of microorganisms and biofilm formation that takes place in natural environments. The establishment of biofilms has been shown to increase the corrosivity of seawater drastically.[97-99] Indeed, the corrosion potential increases to about +300 mV_{SCE} upon the development of a biofilm.[100] This increase in potential is often enough to polarize stainless steels above the critical pitting or crevice potential, depending on the PRE of the alloy. [100, 101]

A second objective of the CREVCORR program discussed above was to develop alternative synthetic seawater chemistry that would better simulate the effect of biofilms during testing in the laboratory.[102] Based on comprehensive electrochemical measurements, the CREVCORR project proposed two possible synthetic seawater compositions. The so-called Chemical Method uses 3.5 wt% NaCl with the addition of 1mM H_2O_2 and 1mM gluconic acid ($C_6H_{12}O_7$). The Biochemical Method involves adding glucose oxidase (GOD) (100 U/L) and 20 mmol/L glucose to either 3.5 wt% NaCl or a simplified version of the ASTM D1141 composition (i.e., NaCl 24.53 $g{\cdot}L^{-1}$, $MgCl_2$ 5.20 $g{\cdot}L^{-1}$, Na_2SO_4 4.09 $g{\cdot}L^{-1}$, $CaCl_2$ 1.16 $g{\cdot}L^{-1}$, KCl 0.695 $g{\cdot}L^{-1}$, $NaHCO_3$ 0.201 $g{\cdot}L^{-1}$) referred to as simplified ASTM Type seawater.[102] Appendix D of the EFC Publication No 60 details a proposal for an ISO standard specification for synthetic biochemical ocean or seawater. Nevertheless, the standard has yet to be published.[103]

ELECTROCHEMICAL TEST METHODS

Electrochemical methods are powerful tools to obtain not only a comparative ranking of localized corrosion performance but also quantitative information regarding pitting and crevice mechanisms. Tests can be conducted without an external polarization at the so-called corrosion potential (E_{Corr}) or under different polarization profiles. E_{Corr} is the potential of a corroding surface in a given electrolyte measured under open-circuit conditions versus a reference electrode.[1] At E_{Corr}, the rate of the sum of the anodic reactions equals that of the cathodic reactions and, thus, the net current is zero. Other experiments with no applied polarization employ a zero-resistance ammeter to measure the current flow between two working electrodes, which can be identical or dissimilar.

Tests conducted under an applied current or potential can be used to quantify critical potentials. Critical potentials include the pitting and crevice potentials (E_P or E_{Crev}, respectively) as well as critical repassivation potentials (E_R or $E_{R,Crev}$ depending on whether the experiments are performed using artificial crevices). Potentiostatic tests, i.e., experiments under a fixed potential, can also provide information regarding the induction time, τ. Additionally, the critical pitting or crevice temperatures can be obtained when multiple electrochemical tests—either at E_{Corr} or employing an external polarization—are performed at different temperatures.

This section describes conventional approaches that have been implemented by researches to quantify localized corrosion resistance, rank alloy families based on performance, and study localized corrosion mechanisms.

Electrochemical test methods with no external polarization

Corrosion Potential Measurements

Oldfield and Sutton showed that the initiation of crevice corrosion of stainless steels is accompanied by a sudden decline in E_{Corr} from values within the passive region to low values around the critical potential (i.e., E_{Crev}). The authors showed that the initial drop was associated with the formation of micro-pitting within the crevice gap, followed by pit coalescence and spreading into a well-developed crevice attack. [24] Haugan et al., for example, recently used E_{Corr} to determine induction times of different super duplex stainless steels (SDSS) as a function of temperature when exposed to natural seawater. [70] Since they are non-destructive, E_{Corr} measurements could also be used to assess the risk of localized corrosion of immersed structures in real-time during field monitoring and, as suggested by Dunn and co-workers, to model the long-term performance of corrosion-resistant alloys.[104]

Standard test methods such as ASTM G48 and G78 can be adapted to include E_{Corr} monitoring to indicate the initiation of localized corrosion.[105] FIG. 6 shows the E_{Corr} of UNS S32750 immersed in 6 wt% $FeCl_3$ (pH = 1.10) as a function of time during a stepwise increase in temperature. The temperature was increased by 5 °C increments every 24-h if the E_{Corr} remained within typical passive potentials, i.e., approximately 0.68 V_{SSE}. The sudden drop in potential at 75 °C marked the initiation of localized corrosion, which was confirmed visually after testing. In this example, the CPT was, thus, defined as 75°C. Others have suggested the use of E_{Corr} monitoring during G48 testing, as an additional pass/fail criteria, which may be especially relevant in quality control test methods such as ASTM A923,[106] and to detect sensitized microstructures.[107]

The Remote Crevice Assembly

First used by Lee[108], the remote crevice assembly implies coupling a creviced specimen to a crevice-free coupon, both made of the same material. The galvanic current flow between specimens is, then, recorded using a zero-resistance ammeter. The coupled potential is monitored concurrently with the net galvanic current as a function of time. The area of the non-creviced sample should be larger than that of the creviced coupon to ensure the cathodic reactions are primarily sustained on the crevice-free side. The choice of area ratio depends on the intended application, and experiments can be done with different anode-cathode ratios to study the possible effects of the cathode area. For instance, in a low conductivity solution, such as the case of condensed water films, the area ratio is expected to be small (e.g., 2:1). In contrast, in full-immersion tests in seawater, the ratio can be quite high (e.g., 300:1).[100]

The remote crevice assembly simulates a real crevice where the crevice-free sample acts as a net cathode and the crevice sample as the net anode. As with any test method based on zero-resistance amperometry (ZRA), both the magnitude and the direction of the current flow carry information about the corrosion process. For this reason, it is crucial to define a sign convention. In this regard, it is common to connect the two working electrodes so that a positive current represents the flow of electrons from the creviced to the crevice-free specimen.[109]

The remote crevice assembly is sensitive to the early stages of crevice corrosion, and it has been used to quantify crevice corrosion initiation and propagation, [110] modeling crevice corrosion of UNS N06625,[111] as well as to determine the effect of biofilms on crevice corrosion of corrosion-resistant alloys. [112] More recently, Martin et al. adapted the remote crevice assembly technique to study the crevice corrosion resistance of Ni-Cr-Mo alloys exposed to seawater. [113]

Visual inspection after exposure is paramount to correlate the observed current trends with the degree of crevice corrosion. Likewise, while there is no international standard regulating the methodology and no consensus on a critical current value to define the initiation of crevice corrosion, the ASTM G71 standard can be used as a guide. [114]

Zero Resistance Amperometry and Electrochemical Noise

Salinas-Bravo and Newman [115] and Garfias [116-119] popularized the use of ZRA to determine critical pitting temperatures of stainless steels. Later, others have employed electrochemical noise (EN) analysis to investigate the crevice corrosion resistance of stainless steels under simulated high-pressure high-temperature oil and gas environments. [109]

As with the remote crevice assembly, ZRA and EN measure the current flow between two working electrodes. Unlike the remote crevice assembly, ZRA and EN require two identical creviced specimens. During ZRA and EN testing, the start of crevice corrosion leads to an increase in current—which can be either positive or negative depending on the electrode that developed crevice attack first—and a drop in coupled potential. A change in sign indicates a reversal in the net anodic or cathodic behavior versus the defined sign convention. FIG. 7a shows the coupled current and potential of creviced UNS S32760 specimens in 6 wt% $FeCl_3$ (pH = 1.10) as a function of temperature during ZRA testing. In this case, the temperature was increased at 0.2 °C/min. The initiation of crevice corrosion was defined as a sustained current above 5 µA after Salinas-Bravo and Newman.[115] In this case, the critical crevice temperature, T_{Crev}, was 41.8 °C. Herein, the nomenclature T_{Crev} is used instead of CCT to indicate the critical temperature was determined using electrochemical means rather than as per ASTM G48.

Unlike ZRA, EN requires a more sophisticated analysis of the results. In this regard, the data can be analyzed in the time domain (i.e., as recorded) or transported to the frequency domain using, e.g., a fast Fourier transformation (FFT) algorithm or the maximum entropy method (MEM). Once transformed into the frequency domain, Power Spectral Density (PSD) plots can be constructed to analyze EN current and potentials as well as to obtain the EN impedance. For a detailed overview of the EN analysis, the work by Cottis [120], as well as the ASTM G199 standard [121], can be consulted.

As with the remote crevice assembly technique, visual inspection after exposure is required to correlate the observed current trends with the degree of crevice corrosion, FIG. 7b. The ASTM G199 standard can be used as a guide.

Electrochemical methods employing an applied polarization

The techniques for evaluating crevice corrosion that employ an applied polarization involve holding or incrementally changing, either in steps or at a fixed scan rate, the potential or current. Some of the more common tests methods, as defined in the ASTM G193 standard, are:

Potentiostatic polarization—a technique for maintaining a constant electrode potential. The current response is measured as a function of time. Different samples can be exposed at different applied potentials (E_{App}).

Galvanostatic technique—a technique wherein an electrode is maintained at a constant current in an electrolyte. The resulting electrode potential is recorded as a function of time. Different samples can be exposed at different applied currents or current densities (I_{App} or i_{App}, respectively).

Potentiostaircase or potentiostep technique—a potentiostep technique for polarizing an electrode in a series of constant potential steps wherein the time duration and potential increments or decrements are equal for each step. Nevertheless, when studying crevice corrosion, the duration of each step can be varied.

Galvanostaircase or galvanostep technique—a galvanostep technique for polarizing an electrode in a series of constant current steps wherein the time duration and current increments or decrements are equal for each step.

Potentiodynamic or potentiokinetic polarization—a technique wherein the potential of an electrode with respect to a reference electrode is varied at a selected rate (e.g., 0.6 V/h) by the application of a current through the electrolyte. When the potential is scanned in a direction so that $E_{App} \geq E_{Corr}$, the result is an anodic polarization curve (i.e., an E-i diagram). Anodic polarization diagrams are used to determine, e.g., E_P and E_{Crev}. The ASTM G5 standard describes a method to conduct a potentiokinetic anodic polarization measurements on stainless steels and nickel alloys, which can also be applied to other alloy families. [122]

Cyclic potentiodynamic polarization—a technique where the applied potential is scanned forward from some low value, typically E_{Corr}, to a high value until reaching a predefined current density (e.g., 5 mA/cm^2) or potential and, then, scanned backward to a predetermined potential or current value. The reverse scan continues until the hysteresis loop closes or until a new corrosion potential is reached. The method is described in ASTM G61.

These techniques are often used alone or combined with varying other environmental factors such as temperature, pH, chloride concentration, etc., as discussed previously. it is important to emphasize that, for a given environment, critical potentials and temperatures are not a property of the metal or alloy, as they are influenced by experimental parameters such as potential and temperature scan rate [14, 123, 124] and the selected current at scan reversal.[125] These and other methods are also described in more detail below.

Potentiostatic electrochemical test methods

Chronoamperometry

Chronoamperometry involves applying either a constant potential or a series of potential steps and recording the resulting current or current density as a function of time. Tests can be performed using

creviced and crevice-free specimens. Chronoamperometry is primarily used to estimate induction times.[126, 127] Nevertheless, chronoamperometry can be used to determine critical temperatures (i.e., T_{Pit} or T_{Crev}) when done as a function of temperature. Repassivation temperatures can also be obtained if the temperature is reduced after pitting or crevice corrosion initiation.

FIG. 8 shows current density as a function of time of a creviced UNS S39274, i.e., a high-W SDSS, immersed in natural seawater during a stepwise increase in temperature followed by a stepped decrease in temperature. The applied potential was +300 mV_{SSE} to simulate the effect of naturally occurring biofilms.[100] During the forward ramp, the temperature was held for 15 days at each step. If no increase in current was observed, the temperature was increased by 5 °C. The ramping continued until an apparent increase in current was observed. The critical crevice temperature, T_{Crev}, was adapted after Steinsmo et al.,[101] as the temperature step where the current density exceeded 25 $\mu A/cm^2$ for at least 4 h. This value was chosen as it corresponded to a marked deviation from the passive current density. Once the current density was reached, the temperature was then decreased in a 7-day period at 2.5 °C steps, until a stable passive behavior was observed. The repassivation temperature was arbitrarily defined as the temperature at which the current density dropped below the 25 $\mu A/cm^2$ threshold, and stable passive current density values were observed.

FIG. 8 and the work of Steinsmo et al.[101] illustrate well the hysteresis that exists between the temperature at which crevice corrosion starts and repassivates. In their earlier work, Steinsmo and coworkers applied a +600 mV_{SCE} potential to simulate chlorinated seawater and a temperature scan rate of 4 °C/24h; a technique often referred to as cyclic thermammetry. [128] In the case of UNS N08367, the authors observed an approximately 50 °C difference between T_{Crev} and $T_{R,\,Crev}$. The difference between T_{Crev} and $T_{R,Crev}$ shown in FIG. 8 was about 8 °C, much lower than the values reported by Steinsmo and coworkers for other corrosion-resistant alloys. [101] The difference in the case of UNS S39274 was attributed to the influence of tungsten.

ASTM F746 Pitting or Crevice Corrosion of Metallic Surgical Implant Materials

The ASTM F746 standard is used to assess the pitting and crevice corrosion resistance of surgical implant materials.[129-131] The localized corrosion resistance is determined based on the critical potential, E_{Crit}, to initiate pitting, crevice corrosion, or both. The primary purpose of the specification is to perform a laboratory screening of materials. Tests are conducted in phosphate-buffered saline (PBS) solution—8.0 $g{\cdot}L^{-1}$ NaCl, 0.2 $g{\cdot}L^{-1}$ KCl, 1.44 $g{\cdot}L^{-1}$ Na_2HPO_4, and 0.24 g·L-1 KH_2PO_4—with a pH between 7.3 and 7.5. The temperature of the electrolyte is set to 37 ± 1 °C to simulate the temperature of the human body. The

standard employs cylindrical specimens that are 6.35 mm in diameter and 20 mm in length. The crevice assembly consists of an inert tapered PTFE collar, 3.18 mm in width. The collar is force-fit into the specimen from the base of the cylinder. FIG. 9 illustrates the ASTM F746 crevice setup.

The procedure can be divided into three steps. Step 1 involves the measurement of a stable corrosion potential for 1-h, referred to as E_1. Step 2 is the stimulation step. The purpose of the stimulation step is to initiate localized corrosion. The applied potential is set at E_{App} = +800 mV_{SCE}, while the duration depends on the current response. If the current density instantly increases above +500 µA/cm^2, the potential is immediately decreased to E_1. If the current generally increases but i < +500 µA/cm^2, the potential is reduced to E_1 after 20s. The test is terminated if there is no sharp increase in current density after 15 minutes.

The last step, Step 3, is called the repassivation step. In Step 3, the applied potential is decreased to E_{App} = E_1. If no repassivation is observed, i.e., the current remains above the passive current density, E_{Crit} is defined as E_{Crit} = E_1. If repassivation occurs, the process is repeated. The new applied potential in Step 3, after the new stimulation step, is set as E_{App}= E_1 + 50 mV. The sequence is continued until no repassivation occurs in Step 3. The assessment entails the quantification of E_{Crit} and a visual confirmation after testing.

Modified ASTM G150 – Potential-independent critical temperature

The ASTM G150 standard is used to determine the so-called potential-independent critical pitting temperature. The tests can be modified to determine the potential-independent critical crevice temperature by employing creviced specimens, as described in ASTM G48 or G78 (FIG. 4). ASTM G150 can also be used to predict the conditions that would result in stable crevice propagation. The test method applies to stainless steels from UNS 31600 to S31254, but it could be extended to other alloy families. Tests are performed in deaerated 1M NaCl (unadjusted pH). The technique implies applying a fixed potential and measure the current response as a function of time. The recommended potential is +700 mV_{SCE}, but other values can be used. A test at +600 or +800 mV_{SCE} can be performed to determine changes in the critical temperature. During testing, the temperature is ramped at 1 °C/min. The potential-independent CPT or CCT is defined as the temperature at which i > 100 µA/cm^{-2} for 60s. Visual confirmation is required at the end of the test to verify the presence of pitting and crevice corrosion. FIG. 10 illustrates a modified ASTM G150 test using a PTFE MCA on UNS S32750. The applied potential was +700 mV_{SCE}, and the CCT varied between 61 and 65 °C.

Potentiokinetic electrochemical test methods

Modified ASTM G61 – Cyclic potentiodynamic polarization

The ASTM G61 standard is arguably the most common electrochemical technique used to determine the relative susceptibility to localized corrosion, namely, pitting or crevice, of stainless steels, cobalt- and some nickel-based alloys. ASTM G61 focuses on crevice-free specimens, but the standard can be modified to study creviced samples. The crevice former is often an MCA that complies with, e.g., ASTM G48. The analysis of the E-i diagrams provides information about the critical crevice and crevice repassivation potentials, E_{Crev} and $E_{R,Crev}$ (E_P and E_R if using crevice-free samples). Likewise, the critical crevice temperature and critical repassivation temperature (T_{Crev} and $T_{R,Crev}$, respectively) can be obtained when multiple experiments are performed at different temperatures. When done on crevice-free specimens, the standard can be used to check one's experimental technique and instrumentation.

As per ASTM G61, experiments are performed in deaerated 3.56 wt% NaCl (neutral pH) at 25 ± 1 °C, but other environments and temperatures can be used. The test is divided into two steps. First, the working electrode is exposed at the corrosion potential for 1-h until a stable E_{Corr} is obtained. The potentiodynamic polarization commences immediately after the 1-h stabilization step. The potential is scanned at 0.6 V/h (0.168 mV/s) in the forward direction until reaching a current density threshold of 5 mA/cm^2. Once the current density threshold is met, the direction of the scan is reversed until the hysteresis loop closes or once reaching a new E_{Corr}. The data is plotted in an E-i diagram, where the current density *i* is presented in logarithmic scale.

There are different ways to determine pitting, crevice, and repassivation potentials from E-i diagrams. According to Sridhar and Cragnolino,[125] E_P can be measured at the inflection point of the E-i plot, while E_R is defined as the potential, in the backward scan, where the current density reaches 2 µA/cm^2. A similar convention can be applied to tests using MCAs to determine E_{Crev} and $E_{R,Crev}$.[70] For creviced specimens, hysteresis, ΔE, is defined as:

$$\Delta E_{Crev} = E_{Crev} - E_{R,Crev} \quad \text{Eq. 9}$$

When evaluating crevice-free samples—where hysteresis is defined as $\Delta E = E_R - E_P$—it is accepted that alloys with large ΔE values are more susceptible to localized corrosion than those with small hysteresis loops.[14]

FIG. 11a and b show two potentiokinetic E-i curves of UNS S32750 in 3.56 wt% NaCl at two different temperatures. Each diagram presents two repetitions to illustrate the test-to-test variability. The E-i curves shown in FIG. 11a and 10b were obtained at 30 and 60 °C, respectively. In FIG. 11a, the sharp increase in current was associated with the transpassive region and, thus, the potential was labeled E_{Trans}. The transpassive region represents the "region of an anodic polarization curve, more positive than the passive potential range, in which there is a significant increase in current density (increased metal oxidation) as the potential becomes more positive." [1] In contrast, a large hysteresis loop was obtained at 60 °C, FIG. 11b. The forward scan in FIG. 11b also reached high positive values, but crevice corrosion occurred upon scan reversal as confirmed visually. The high ΔE value suggested that the driving force for crevice corrosion was large.[46] FIG. 11c presents an E vs. temperature plot, constructed from a series of cyclic anodic polarization curves performed at different temperatures. The critical crevice repassivation temperature, $T_{R,Crev}$, was 56 °C. FIG. 11c also illustrates that the critical temperature has a well-defined value, as suggested by Brigham and Tozer [47, 48], which in this case was within 5 °C and limited by temperature interval chosen for the tests.

Precision and bias in ASTM G61 testing

The ASTM G61 standard shows the precision of the test method based on interlaboratory testing. An investigator's data should fall within the range of ±2 standard deviations since this includes 95 % of all data provided random variations are the only source of error. No information is available on the repeatability when one laboratory conducts several identical tests. Crevice corrosion under gaskets may lead to erroneous results. Researchers have also found that the scatter in E_P and E_{Crev} is much larger than the scatter in E_R and $E_{R,\ Crev}$. [104, 132, 133] For example, the limited experimental data suggest a scatter in $E_{R,Crev}$ for type 316L stainless steel, and UNS N09925 of about 100 mV. [104]

ASTM G192 – Tsujikawa-Hisamatsu Electrochemical (THE) technique

Adapted from the work of Tsujikawa and Hisamatsu on stainless steels, the ASTM G192 standard [134] is a complex technique that involves potentiodynamic, galvanostatic, and potentiostatic steps.[135] The test has been used to study the crevice [84, 136, 137] and pitting [138] corrosion susceptibility of highly-alloyed nickel alloys. The ASTM G192 technique is used to determine the $E_{R,Crev}$ of corrosion-resistant alloys. It is understood that an alloy will not develop crevice corrosion below $E_{R,Crev}$ under the tested conditions (i.e., electrolyte composition, pH, and temperature). Although the ASTM G192 method was developed for alloy C22, it applies to any corrosion-resistant alloy. The standard suggests the use of a

PFTE tape-covered ceramic MCA and a torque of 3.4 N·m. The test can be modified to measure the critical crevice repassivation temperature, $T_{R,Crev}$ if done at various temperatures.

The tests can be done in any electrolyte, albeit the method was developed using a deaerated 1M NaCl. The recommended test temperature for alloy C22 is 90 °C, but lower temperatures can be chosen for less corrosion-resistant metals and alloys. The procedure can be divided into three steps, as follows. The potentiodynamic (PD) step commences after a 1-h E_{Corr} stabilization period. During the PD step, the potential is scanned in the forward anodic direction at 0.6 V/h (0.168 mV/s) until a pre-set current is reached (e.g., 2 μA/cm^2 for alloy C22). The galvanostatic (GS) step starts after reaching the current density threshold. In the GS period, the pre-set current is kept constant for 2-h, while the potential is recorded as a function of time. The goal of the GS step is to develop and grow crevice attack if any develops. After the 2-h GS period, the potential is decreased at 10 mV intervals. The duration of each step is 2-h and the current recorded versus time. $E_{R,Crev}$ is defined as the highest potential for which the current does not increase with time. The presence and extent of crevice corrosion are verified using visual inspection after testing.

Precision and bias in ASTM G192

Under some testing conditions, results from this method may be comparable to results from ASTM G61. The current Tsujikawa and Hisamatsu electrochemical test method is meant to be a complement to ASTM G61. The *THE* test method may produce crevice corrosion in conditions where cyclic potentiodynamic polarizations have limitations caused by transpassive dissolution.

Results of an interlaboratory program showed that the overall crevice repassivation potential for alloy C22 in 1 M NaCl at 90°C was -107 $mV_{SSE,}$ and the standard deviation was 10.0 mV. This low standard deviation suggests that the measurement of the repassivation potential using the PD-GS-PS test method is highly reproducible. For more details, ASTM G192 should be consulted.

Potentiodynamic-Galvanostatic-Potentiodynamic technique

Although the Tsujikawa-Hisamatsu electrochemical technique circumvents the limitations of the ASTM G61 method for highly-corrosion resistant alloys that would otherwise present transpassive dissolution before crevice corrosion, the method is time-consuming and challenging to automate. [136, 139] For this reason, Mishra and Frankel developed a simplified version of the ASTM G192 standard that replaces the PS step by a PD polarization.[137] In the so-called PD-GS-PD technique, the potential is first scanned at 0.6 V/h (0.168 mV/s) until the predefined current density threshold. The threshold current density is,

then, applied for 2-h to promote the initiation and propagation of crevice corrosion. After the 2-h GS step, the potential is reverted at a scan rate of 0.6 V/h (0.168 mV/s) until the hysteresis loop closes. The $E_{R,Crev}$ is defined as a cross-over potential.

The PD-GS-PD method has been successfully used not only on nickel alloys [64, 84, 139-142] but also stainless steels with varying degrees of corrosion resistance.[32, 33] FIG. 12 illustrates an E-i plot as well as the E vs. time curve recorded during the GS step of UNS N06059 (alloy 59) in 10 M Cl^- at two different temperatures, as indicated. As seen in FIG. 12, crevice corrosion did not occur at 40 °C, as suggested by the lack of a positive hysteresis loop, which was later confirmed visually (not shown). Crevice corrosion was evident at 90 °C, and the hysteresis loop was about ΔE = 200 mV. FIG. 12c shows the extent of the crevice attack after PD-GS-PD testing.

Crevice corrosion repassivation by cooling

Hornus and coworkers have recently adapted the PD-GS-PD technique to study crevice repassivation by cooling. The authors named the technique PD-GS-PD-(PS + Cooling), which was designed to determine $T_{R,Crev}$ values of nickel alloys. [30] First, the temperature of the electrolyte is set to 90 °C. After reaching the desired initial temperature, the procedure involves five steps. Step 1 (PD) consists of an anodic potentiodynamic polarization at 0.6 V/h (0.168 mV/s) until the anodic current density reaches 20 μA/cm^2. In Step 2 (GS), the applied current is set at 20 μA/cm^2 for 4-h. Given that the current drops instantaneously upon removal of the GS, Step 3 involves a potentiodynamic polarization at 0.06V/h (0.0168 mV/s) until the current density reaches ≥ 20 μA/cm^2. In Step 4 (PS), the last potential of Step 3 is applied for at least 2-h to produce sufficient crevice corrosion to obtain a conservative $T_{R,Crev}$ value. Likewise, Step 4 was designed to ensure a relatively low current density so that the drop in current during Step 5 can be attributed to the cooling effect exclusively. Lastly, the temperature is decreased while holding the PS polarization at a given cooling rate of, e.g., 3.33 or 33.3 °C/h, until the current reaches typical passive current density values. The $T_{R,Crev}$ is determined once i = 1 μA/cm^2. FIG. 13 illustrates Step 5 applied to UNS N06625 (alloy 625) and N10362 (alloy Hybrid B-C1) in 0.1M NaCl at two different cooling rates. In this example, the $T_{R,Crev}$ of alloy Hybrid B-C1 was approximately 60 °C while that of alloy 625 was approximately 35 °C.

Although applying the PD-GS-PD-(PS + Cooling) technique to, e.g., stainless steels and nickel alloys with relatively low PRE (e.g., PRE < 40 [80]) might be excessively complicated, the method can be used to quantify the critical crevice repassivation temperature of highly corrosion-resistant nickel-alloys, which cannot be done using other conventional tests methods.

Depassivation pH and the critical crevice solution

As proposed by Oldfield and Sutton, the depassivation pH (pHd) is defined as the pH where a metal or alloy does not exhibit any passivity. [21, 24] The pHd value is associated with the critically acidic environment that develops inside a crevice, as discussed above. In this regard, Oldfield and Sutton referred to the solution that causes the permanent breakdown of the passive film within a crevice and the rapid propagation of the attack as critical crevice solution (CCS).[21, 24] According to the authors, the CCS is defined in terms of pH (i.e., the pHd) and chloride concentration. The pHd and CCS can be obtained experimentally using polarization curves in crevice-like environments as a function of solution pH and chloride concentration. Malik et al. [87] and Okayama et al. [143], e.g., determined the CCS of a considerable number of CRAs of increasing PRE. Polarization experiments can be performed adapting ASTM G5 and G61 or by monitoring the potential of a specimen under galvanostatic conditions, while simultaneously decreasing the pH by the addition of HCl. There are, however, no broadly accepted standard procedures to determine CCS.

CONCLUSIONS

This chapter summarized the most common electrochemical and non-electrochemical methods to study crevice corrosion. Other approaches such as multi-microelectrode array testing and electrochemical methods that can quantify local electrochemical reactions with high spatial resolution, were not covered. In closing, it is important to emphasize that the choice of methodology depends on the problem being study. In this regard, all techniques have advantages and disadvantages that need to be considered carefully. Indeed, often short-term accelerated laboratory tests should be combined with long-term exposure evaluations to validate critical parameters such as induction times, crevice propagation rates, and critical temperatures. The ample literature cited herein can be consulted for more detailed discussions on crevice corrosion mechanisms.

ACKNOWLEDGEMENTS

We thank Dr. Ke Wang, Cristian Torres, and Adam Cianfrini for their support in producing the figures for this publication.

TERMS AND DEFINITIONS

CCS	Critical crevice solution.
CCT	Critical crevice temperature, as determined by ASTM G48
CPT	Critical pitting temperature, as determined by ASTM G48.
CRA	Corrosion-resistant alloy.
DSMCA	Disc spring multiple crevice assembly
E_{App}	Applied potential.
E_{Crev}	Critical crevice potential (crevice initiation potential).
E_{Crit}	Critical potential as defined by the critical acidification model.
E_{Corr}	Corrosion potential
E^*_{Corr}	Corrosion potential in a simulated crevice electrolyte.
E_{ihn}	Overpotential to reflect the contribution of the presence of inhibitors in the solution.
E_P	Critical pitting potential (pitting corrosion initiation)
E_R	Repassivation potential.
$E_{R,Crev}$	Crevice repassivation potential.
g	Crevice gap
I or I	Current or current density
I_{App} or i_{App}	Applied current or current density, respectively.
i_{pass}	Passive current density.
L	crevice length measured as the distance from the crevice mouth.
MCA	Multiple-crevice assembly
pHd	Depassivation pH.
PCTFE	Polychlorotrifluoroethylene
PRE	Pitting Resistant Equivalent.
PTFE	Polytetrafluoroethylene
PVDF	Polyvinylidene difluoride
SCE	Saturated Calomel Electrode.
SSE	Silver/Silver Chloride Electrode.
T_{Crev}	Critical crevice temperature measured using electrochemical methods.
T_{Crit}	Critical temperature (either pitting or crevice).
T_{Pit}	Critical pitting temperature measured using electrochemical methods.
$T_{R,Crev}$	Critical crevice repassivation temperature measured using electrochemical methods.
x	Diffusion path
x·i	Galvele's pitting or crevice stability product.
ZRA	Zero resistance amperometry.

η	Polarization needed to reach the critical xi value
Φ	The electrical potential induced by the migration of the aggressive anions to the crevice.
τ	Induction or incubation time.

REFERENCES

1. NACE/ASTM G193-12d, *Standard Terminology and Acronyms Relating to Corrosion.* West Conshohocken, PA; ASTM International, 2012.
2. Kelly, R.G., "Crevice Corrosion," *ASM Handbook, Volume 13A: Corrosion: Fundamentals, Testing, and Protection*, S.D. Cramer and B.S. Covino, Jr., Eds., ASM International: Metals Park, OH, 2003, pp. 242-247.
3. Betts, A.J. and L.H. Boulton, "Crevice corrosion: review of mechanisms, modelling, and mitigation," *British Corrosion Journal*, Vol. 28, No. 4, 1993, pp. 279-296.
4. Gallagher, P., R.E. Malpas, and E.B. Shone, "Corrosion of stainless steels in natural, transported, and artificial seawaters," *British Corrosion Journal*, Vol. 23, No. 4, 1988, pp. 229-233.
5. Schlain, D. and C.B. Kenahan, "The role of crevices in decreasing the passivity of titanium in certain solutions," *Corrosion*, Vol. 12, No. 8, 1956, pp. 422t-426t.
6. Standish, T.E., et al., "Crevice Corrosion of Grade-2 Titanium in Saline Solutions at Different Temperatures and Oxygen Concentrations," *Journal of The Electrochemical Society*, Vol. 164, No. 13, 2017, pp. C788-C795.
7. Brown, B.F., "Concept of the Occluded Corrosion Cell," *Corrosion*, Vol. 26, No. 8, 1970, pp. 249-250.
8. Laycock, N.J., J. Stewart, and R.C. Newman, "The initiation of crevice corrosion in stainless steels," *Corrosion Science*, Vol. 39, No. 10-11, 1997, pp. 1791-1809.
9. Galvele, J.R., "Tafel's law in pitting corrosion and crevice corrosion susceptibility," *Corrosion Science*, Vol. 47, No. 12, 2005, pp. 3053-3067.
10. Mears, R.B. and U.R. Evans, "Corrosion at contact with glass," *Transactions of the Faraday Society*, Vol. 30, 1934, pp. 417-423.
11. Kearns, J.R., M.J. Johnson, and J.F. Grubb. "Accelerated Corrosion in Dissimilar Metal Crevices," CORROSION/86, Paper 228, Houston, TX: NACE International 1986.
12. Frankel, G.S. and N. Sridhar, "Understanding localized corrosion," *Materials Today*, Vol. 11, No. 10, 2008, pp. 38-44.
13. ASTM A480/A480M-18, *Standard Specification for General Requirements for Flat-Rolled Stainless and Heat-Resisting Steel Plate, Sheet, and Strip.* West Conshohocken, PA; ASTM International, 2018.
14. Wilde, B.E. and E. Williams, "The use of current/voltage curves for the study of localized corrosion and passivity breakdown on stainless steels in chloride media," *Electrochimica Acta*, Vol. 16, No. 11, 1971, pp. 1971-1985.
15. Uhlig, H.H., "Pitting of Stainless Steels," *Transactions of AIME*, Vol. 140, 1940, pp. 387-432.

16. Galvele, J.R., "Pitting corrosion," *Corrosion: Aqueous processes and passive films*, J.C. Scully, Ed., Academic Press: London, U.K., 1983, pp. 1-57.

17. Rosenfeld, I.L. and I.S. Danilov, "Electrochemical aspects of pitting corrosion," *Corrosion Science*, Vol. 7, No. 3, 1967, pp. 129-142.

18. Galvele, J.R., "Transport Processes and the Mechanism of Pitting of Metals," *Journal of The Electrochemical Society*, Vol. 123, No. 4, 1976, pp. 464-474.

19. Galvele, J.R., "Transport processes in passivity breakdown—II. Full hydrolysis of the metal ions," *Corrosion Science*, Vol. 21, No. 8, 1981, pp. 551-579.

20. Gravano, S.M. and J.R. Galvele, "Transport processes in passivity breakdown—III. Full hydrolysis plus ion migration plus buffers," *Corrosion Science*, Vol. 24, No. 6, 1984, pp. 517-534.

21. Oldfield, J.W. and W.H. Sutton, "Crevice Corrosion of Stainless Steels: I. A Mathematical Model," *British Corrosion Journal*, Vol. 13, No. 1, 1978, pp. 13-22.

22. Oldfield, J.W., "Test techniques for pitting and crevice corrosion resistance of stainless steels and nickel-base alloys in chloride-containing environments," *International Materials Reviews*, Vol. 32, No. 1, 1987, pp. 153-172.

23. Carranza, R.M., M.A. Rodriguez, and R.B. Rebak, "Effect of fluoride ions on crevice corrosion and passive behavior of alloy 22 in hot chloride solutions," *Corrosion*, Vol. 63, No. 5, 2007, pp. 480-490.

24. Oldfield, J.W. and W.H. Sutton, "Crevice Corrosion of Stainless Steels: II. Experimental studies," *British Corrosion Journal*, Vol. 13, No. 3, 1978, pp. 104-111.

25. Alkire, R. and D. Siitari, "Initiation of Crevice Corrosion. II.--Mathematical Model for Aluminum in Sodium Chloride Solutions," *Journal of the Electrochemical Society*, Vol. 129, No. 3, 1982, pp. 488-496.

26. Walton, J.C., "Mathematical modeling of mass transport and chemical reaction in crevice and pitting corrosion," *Corrosion Science*, Vol. 30, No. 8-9, 1990, pp. 915-928.

27. Keitelman, A.D., S.M. Gravano, and J.R. Galvele, "Localized acidification as the cause of passivity breakdown of high purity zinc," *Corrosion Science*, Vol. 24, No. 6, 1984, pp. 535-545.

28. Rodriguez, M.A., "Inhibition of localized corrosion in chromium containing stainless alloys," *Corrosion Reviews*, Vol. 30, No. 1-2, 2012, pp. 19-32.

29. Newman, R.C., et al., "An experimental confirmation of the pitting potential model of galvele," *Corrosion Sci.*, Vol. 28, No. 5, 1988, pp. 471-477.

30. Hornus, E.C., et al., "Crevice Corrosion Repassivation of Ni-Cr-Mo Alloys by Cooling," *Corrosion*, Vol. 75, No. 6, 2019, pp. 604-615.

31. Srinivasan, J. and R.G. Kelly, "On a Recent Quantitative Framework Examining the Critical Factors for Localized Corrosion and Its Impact on the Galvele Pit Stability Criterion," *Corrosion*, Vol. 73, No. 6, 2017, pp. 613-633.

32. Kappes, M.A., et al., "Use of the Critical Acidification Model to Estimate Critical Localized Corrosion Potentials of Duplex Stainless Steels," *Corrosion*, Vol. 73, No. 1, 2017, pp. 31-40.

33. Hornus, E.C., et al., "Comparative Study of the Crevice Corrosion Resistance of UNS S30400 and UNS S31600 Stainless Steels in the Context of Galvele's Model," *Corrosion*, Vol. 73, No. 1, 2016, pp. 41-52.

34. Galvele, J.R., J.B. Lumsden, and R.W. Staehle, "Effect of Molybdenum on the Pitting Potential of High Purity 18% Cr Ferritic Stainless Steels," *Journal of The Electrochemical Society*, Vol. 125, No. 8, 1978, p. 1204.

35. Bocher, F., R. Huang, and J.R. Scully, "Prediction of Critical Crevice Potentials for Ni-Cr-Mo Alloys in Simulated Crevice Solutions as a Function of Molybdenum Content," *Corrosion*, Vol. 66, No. 5, 2010, pp. 055002-055002-15.

36. Martínez, P.A., et al. "Crevice Corrosion Resistance of Super-Austenitic and Super-Duplex Stainless Steels in Chloride Solutions.," CORROSION/15, paper no. 5740, Dallas, Texas: NACE International 2015.

37. Wood, G.C., et al., "The Role of Flaws in Breakdown of Passivity Leading to Pitting of Aluminum and Crevice Corrosion of Stainless Steel," *Passivity of metals*, R.P. Frankenthal and W.H. Sutton, Eds., The Electrochemical Society: New Jersey, U.S., 1978, pp. 973-988.

38. Stockert, L. and H. Boehni. "Metastable pitting processes and crevice corrosion on stainless steels," H.S. Isaacs, et al., Eds., Advances in Localized Corrosion, Paper NACE-9, Orlando, FL: NACE International 1987, pp. 467-473.

39. Pickering, H.W., "The significance of the local electrode potential within pits, crevices and cracks," *Corrosion Science*, Vol. 29, No. 2, 1989, pp. 325-341.

40. Brossia, C.S. and G.A. Cragnolino, "Effect of environmental variables on localized corrosion of carbon steel," *Corrosion*, Vol. 56, No. 5, 2000, pp. 505-514.

41. Suzuki, T., M. Yamabe, and Y. Kitamura, "Composition of Anolyte within Pit Anode of Austenitic Stainless-Steels in Chloride Solution," *Corrosion*, Vol. 29, No. 1, 1973, pp. 18-22.

42. Mankowski, J. and Z. Szklarskasmialowska, "Studies on Accumulation of Chloride-Ions in Pits Growing during Anodic Polarization," *Corrosion Science*, Vol. 15, No. 8, 1975, pp. 493-501.

43. Li, T., J.R. Scully, and G.S. Frankel, "Localized Corrosion: Passive Film Breakdown vs. Pit Growth Stability: Part IV. The Role of Salt Film in Pit Growth: A Mathematical Framework," *Journal of The Electrochemical Society*, Vol. 166, No. 6, 2019, pp. C115-C124.

44. Li, T., J.R. Scully, and G.S. Frankel, "Localized Corrosion: Passive Film Breakdown vs. Pit Growth Stability: Part III. A Unifying Set of Principal Parameters and Criteria for Pit Stabilization and Salt Film Formation," *Journal of The Electrochemical Society*, Vol. 165, No. 11, 2018, pp. C762-C770.

45. Li, T., J.R. Scully, and G.S. Frankel, "Localized Corrosion: Passive Film Breakdown vs Pit Growth Stability: Part II. A Model for Critical Pitting Temperature," *Journal of The Electrochemical Society*, Vol. 165, No. 9, 2018, pp. C484-C491.

46. Frankel, G.S., T. Li, and J.R. Scully, "Perspective—Localized Corrosion: Passive Film Breakdown vs Pit Growth Stability," *Journal of The Electrochemical Society*, Vol. 164, No. 4, 2017, pp. C180-C181.

47. Brigham, R.J., "Temperature as a Crevice Corrosion Criterion," *Corrosion*, Vol. 30, No. 11, 1974, pp. 396-398.

48. Brigham, R.J. and E.W. Tozer, "Temperature as a Pitting Criterion," *Corrosion*, Vol. 29, No. 1, 1972, pp. 33-36.

49. Kolts, J. and N. Sridhar, "Temperature Effects in Localized Corrosion," *Corrosion of Nickel-Base Alloys*, R.C. Scarberry, Ed., ASM International: Metals Park, OH, 1984, pp. 191-198.

50. Qvarfort, R., "CRITICAL PITTING TEMPERATURE-MEASUREMENTS OF STAINLESS-STEELS WITH AN IMPROVED ELECTROCHEMICAL METHOD," *Corrosion Sci.*, Vol. 29, No. 8, 1989, pp. 987-993.

51. Garner, A., "Materials Selection for Bleached Pulp Washers.(Reprint)," *Pulp Paper Can.*, Vol. 82, No. 12, 1981, p. 12.

52. Pickering, H.W., "The role of electrode potential distribution in corrosion processes," *Materials Science and Engineering: A*, Vol. 198, No. 1-2, 1995, pp. 213-223.

53. Frankel, G., et al., "Localised corrosion: general discussion," *Faraday Discuss*, Vol. 180, 2015, pp. 381-414.

54. Frankel, G.S., "Pitting Corrosion of Metals: a review of the critical factors.," *Journal of The Electrochemical Society*, Vol. 145, No. 6, 1998, p. 2186.

55. Newman, R.C., "2001 W.R. Whitney Award Lecture: Understanding the corrosion of stainless steel," *Corrosion*, Vol. 57, No. 12, 2001, pp. 1030-1041.

56. Ijsseling, F.P., "Electrochemical Methods in Crevice Corrosion Testing: Report prepared for the European Federation of Corrosion Working Party 'Physico-chemical testing methods of corrosion: Fundamentals and applications'," *British Corrosion Journal*, Vol. 15, No. 2, 1980, pp. 51-69.

57. Kain, R.M., "Electrochemical measurement of the crevice corrosion propagation resistance of stainless steels: effect of environmental variables and alloy content," *Materials performance*, Vol. 23, No. 2, 1984, pp. 24-30.

58. Kain, R.M., "Crevice corrosion testing in natural seawater. Significance and use of multiple crevice assemblies," *Journal of Testing and Evaluation*, Vol. 18, No. 5, 1990, pp. 309-318.

59. Kruger, J. and K. Rhyne, "Current understanding of pitting and crevice corrosion and its application to test methods for determining the corrosion susceptibility of nuclear waste metallic containers," *Nuclear and Chemical Waste Management*, Vol. 3, No. 4, 1982, pp. 205-227.

60. Anderson, D.B., "Statistical Aspects of Crevice Corrosion in Seawater," *Galvanic and Pitting Corrosion—Field and Laboratory Studies*, R. Baboian, et al., Eds., ASTM STP 576, ASTM International: West Conshohocken, PA, 1976, pp. 231-242.

61. Kain, R.M. "Seawater Testing to Assess the Crevice Corrosion Resistance of Stainless Steel and Related Alloys," 12th International Corrosion Congress, Vol. 3B: NACE International, 19-24 September 1993, pp. 1889-1990.

62. Kain, R.M., "Evaluating Crevice Corrosion," *ASM Handbook, Volume 13A: Corrosion: Fundamentals, Testing, and Protection*, S.D. Cramer and B.S. Covino, Jr., Eds., ASM International: Metals Park, OH, 2003, pp. 549-561.

63. ASTM G48-11, *Standard Test Methods for Pitting and Crevice Corrosion Resistance of Stainless Steels and Related Alloys by Use of Ferric Chloride Solution.* West Conshohocken, PA; ASTM International, 2011.

64. Giordano, C.M., et al., "Crevice corrosion testing methods for measuring repassivation potential of alloy 22," *Corrosion Engineering, Science and Technology*, Vol. 46, No. 2, 2013, pp. 129-133.

65. "<NACE-98158_PRINTED.pdf>."

66. Shan, X. and J.H. Payer, "Effect of Polymer and Ceramic Crevice Formers on the Crevice Corrosion of Ni-Cr-Mo Alloy 22," *Corrosion*, Vol. 66, No. 10, 2010, pp. 1050051-14.

67. Espelid, B., "Chapter 2: Objectives and background," *EFC-60. Methodology of crevice corrosion testing for stainless steels in natural and treated seawaters*, U. Kivisäkk, B. Espelid, and D. Féron, Eds., Maney Publishing: Wakefield, UK, 2010, pp. 8-11.

68. European Federation of Corrosion Publications, *EFC-60. Methodology of crevice corrosion testing for stainless steels in natural and treated seawaters*, ed. U. Kivisäkk, B. Espelid, and D. Féron. 2010, Wakefield, UK: Maney Publishing.

69. Espelid, B., "Chapter 4: Crevice formers for specimens of plate material," *EFC-60. Methodology of crevice corrosion testing for stainless steels in natural and treated seawaters*, U. Kivisäkk, B. Espelid, and D. Féron, Eds., Maney Publishing: Wakefield, UK, 2010, pp. 17-20.

70. Haugan, E.B., et al., "Effect of Tungsten on the Pitting and Crevice Corrosion Resistance of Type 25Cr Super Duplex Stainless Steels," *Corrosion*, Vol. 73, No. 1, 2017, pp. 53-67.

71. Kivisäkk, U.H., "Relation of room temperature creep and microhardness to microstructure and HISC," *Materials Science and Engineering: A*, Vol. 527, No. 29-30, 2010, pp. 7684-7688.

72. He, X., J.J. Noël, and D.W. Shoesmith, "Temperature Dependence of Crevice Corrosion Initiation on Titanium Grade-2," *Journal of The Electrochemical Society*, Vol. 149, No. 9, 2002.

73. Jakupi, P., J.J. Noel, and D.W. Shoesmith, "Crevice corrosion initiation and propagation on Alloy-22 under galvanically-coupled and galvanostatic conditions," *Corrosion Science*, Vol. 53, No. 10, 2011, pp. 3122-3130.

74. He, X., J.J. Noël, and D.W. Shoesmith, "Crevice corrosion damage function for grade-2 titanium of iron content 0.078wt% at 95°C," *Corrosion Science*, Vol. 47, No. 5, 2005, pp. 1177-1195.

75. Mathiesen, T. and A. Anderko. "Challenges in Pre-Qualification Corrosion Testing of CRAs based on ASTM G48," CORROSION/14, paper no. 4272, Paper 4272, San Antonio, TX: NACE International 2014.

76. Garner, A., "Crevice Corrosion of Stainless-Steels in Sea-Water - Correlation of Field Data with Laboratory Ferric-Chloride Tests," *Corrosion*, Vol. 37, No. 3, 1981, pp. 178-184.

77. Tsujikawa, S., K. Kudo, and H. Ogawa. "A New Test for Predicting Pitting Corrosion Resistance of CRA's in Sour Environments," CORROSION/88, Paper 65, St. Louis, MO: NACE International 1988.

78. Wensley, D.A., R.C. Reid, and H. Dykstra. "Corrosion of Nickel-Based Alloys in Chlorine Dioxide Washer Service," CORROSION/90, Paper 537, Houston, TX: NACE International 1990.

79. DeForce, B.S. "Comments on ASTM G48 - Standard Test Methods for Pitting and Crevice Corrosion Resistance of Stainless Steels and Related Alloys by Use of Ferric Chloride Solution," CORROSION/16, Paper 7198, Vancouver, British Columbia, Canada: NACE International, 6-10 March 2016.

80. Skar, J.I. and S. Olsen, "A Review of Materials Application Limits in NORSOK M-001 and ISO 21457," *Corrosion*, Vol. 73, No. 6, 2017, pp. 655-665.

81. Postlethwaite, J., "Electrochemical Tests for Pitting and Crevice Corrosion Susceptibility," *Canadian Metallurgical Quarterly*, Vol. 22, No. 1, 1983, pp. 133-141.

82. Streicher, M.A., "Development of Pitting Resistant Fe-Cr-Mo Alloys," *Corrosion*, Vol. 30, No. 3, 1974, pp. 77-91.

83. Lau, P. and J. Bernhardsson, "Electrochemical Techniques for the Study of Pitting and Crevice Corrosion Resistance of Stainless Steels," *Electrochemical Techniques for Corrosion Engineering*, R. Baboian, Ed., NACE International: Houston, TX, 1977.

84. Ortiz, M.R., et al., "Determination of the Crevice Corrosion Stabilization and Repassivation Potentials of a Corrosion-Resistant Alloy," *Corrosion*, Vol. 66, No. 10, 2010, pp. 105002-1-12.

85. Garner, A., "Thiosulfate Corrosion in Paper-Machine White Water," *Corrosion*, Vol. 41, No. 10, 1985, pp. 587-591.

86. Renner, M., et al., "Temperature as a pitting and crevice corrosion criterion in the FeCl3 test," *Werkstoffe und Korrosion*, Vol. 37, No. 1, 1986, pp. 183-190.

87. Malik, A.U., et al., "The Effect of Dominant Alloy Additions on the Corrosion Behavior of Some Conventional and High-Alloy Stainless-Steels in Seawater," *Corrosion Science*, Vol. 37, No. 10, 1995, pp. 1521-1535.

88. Lorentz, K. and G. Medawar, "Über das Korrosionsverhalten austenitischer Chrom-Nickel-(Molybd än-) Stähle mit und ohne Stickstoffzusatz unter besonderer Berücksichtigung ihrer Beanspruchbarkeit in chloridhaltigen Lösungen.," *Tyssenforschung*, Vol. 1, No. 3, 1969, pp. 97-108.

89. Jargelius-Pettersson, R.F.A., "Application of the pitting resistance equivalent concept to some highly alloyed austenitic stainless steels," *Corrosion*, Vol. 54, No. 2, 1998, pp. 162-168.

90. NORSOK M-001, *Materials selection.* Lysaker, Norway; Standards Norway, 2014.

91. ISO 21457:2010, *Petroleum, petrochemical and natural gas industries -- Materials selection and corrosion control for oil and gas production systems.* Geneva, Switzerland; International Organization for Standardization, 2010.

92. Klapper, H.S., N.S. Zadorozne, and R.B. Rebak, "Localized Corrosion Characteristics of Nickel Alloys: A Review," *Acta Metallurgica Sinica (English Letters)*, Vol. 30, No. 4, 2017, pp. 296-305.

93. Brigham, R.J., "Pitting and Crevice Corrosion Resistance of 18% Cr Stainless Steels," *Materials Performance*, Vol. 13, No. 11, 1974, pp. 29-31.

94. Qvarfort, R., "New electrochemical cell for pitting corrosion testing," *Corrosion Science*, Vol. 28, No. 2, 1988, pp. 135-140.

95. Dean, S.W., *Research Report on Interlaboratory Test Program Results for ASTM G48 Standard Test Method for Pitting and Crevice Corrosion Resistance of Stainless Steels and Related Alloys by Use of the Ferric Chloride Solution - Methods E and F.* 2002, ASTM International: West Conshohocken, PA.

96. ASTM D1141-98, *Standard Practice for the Preparation of Substitute Ocean Water.* West Conshohocken, PA; ASTM International, 2013.

97. Salvago, G. and L. Magagnin, "Biofilm Effect on the Cathodic and Anodic Processes on Stainless Steel in Seawater Near the Corrosion Potential: Part 1—Corrosion Potential," *Corrosion*, Vol. 57, No. 8, 2001, pp. 680-692.

98. Salvago, G. and L. Magagnin, "Biofilm Effect on the Cathodic and Anodic Processes on Stainless Steel in Seawater Near the Corrosion Potential—Part 2: Oxygen Reduction on Passive Metal," *Corrosion*, Vol. 57, No. 9, 2001, pp. 759-767.

99. Machuca, L.L., S.I. Bailey, and R. Gubner, "Systematic study of the corrosion properties of selected high-resistance alloys in natural seawater," *Corrosion Science*, Vol. 64, No. 1, 2012, pp. 8-16.

100. Steinsmo, U., T. Rogne, and J. Drugli, "Aspects of testing and selecting stainless steels for seawater applications," *Corrosion*, Vol. 53, No. 12, 1997, pp. 955-964.

101. Steinsmo, U., et al., "Critical Crevice Temperature for High-Alloyed Stainless Steels in Chlorinated Seawater Applications," *Corrosion*, Vol. 53, No. 1, 1997, pp. 26-32.

102. Féron, D., V. l'Hostis, and M. Roy, "Chapter 6: Formulation of new synthetic seawater for aerobic environment," *EFC-60. Methodology of crevice corrosion testing for stainless steels in natural and treated seawaters*, U. Kivisäkk, B. Espelid, and D. Féron, Eds., Maney Publishing: Wakefield, UK, 2010, pp. 30-43.

103. European Federation of Corrosion, "Appendix D: ISO proposal for synthetic biochemical seawater," *EFC-60. Methodology of crevice corrosion testing for stainless steels in natural and treated seawaters*, U. Kivisäkk, B. Espelid, and D. Féron, Eds., Maney Publishing: Wakefield, UK, 2010, pp. 105-109.

104. Dunn, D.S., G.A. Cragnolino, and N. Sridhar, "An electrochemical approach to predicting long-term localized corrosion of corrosion-resistant high-level waste container materials," *Corrosion*, Vol. 56, No. 1, 2000, pp. 90-104.

105. Torres, C., et al. "Effect of W on Phase Transformation Kinetics and its Correlation with Localized Corrosion Resistance for UNS S39274," CORROSION 2019, Paper 13233, Houston, TX: NACE International, 24-28 March 2019.

106. ASTM A923-14, *Standard Test Methods for Detecting Detrimental Intermetallic Phase in Duplex Austenitic/Ferritic Stainless Steels.* West Conshohocken, PA; ASTM International, 2014.

107. Iannuzzi, M., A.H. Qvale, and A. Fjeldly, *Rapid non-destructive evaluation of the degree of sensitization in stainless steels and nickel based alloys*. 2019: U.S.

108. Lee, T., "A Method for Quantifying the Initiation and Propagation Stages of Crevice Corrosion," *Electrochemical Corrosion Testing*, F. Mansfeld and U. Bertocci, Eds., ASTM STP 727-EB, ASTM International: West Conshohocken, PA, 1981, pp. 43-68.

109. Iannuzzi, M., et al., "Determination of the Critical Pitting Temperature of Martensitic and Supermartensitic Stainless Steels in Simulated Sour Environments Using Electrochemical Noise Analysis," *Corrosion*, Vol. 66, No. 4, 2010, pp. 0450031-8.

110. Kain, R.M. and T.S. Lee, "Recent Developments in Test Methods for Investigating Crevice Corrosion," *Laboratory Corrosion Tests and Standards*, G. Haynes and R. Baboian, Eds., ASTM STP 866-EB, ASTM International: West Conshohocken, PA, 1985, pp. 299-323.

111. Lillard, R.S. and J.R. Scully, "Modeling of the Factors Contributing to the Initiation and Propagation of the Crevice Corrosion of Alloy 625," *Journal of The Electrochemical Society*, Vol. 141, No. 11, 1994, pp. 3006-3015.

112. Zhang, H.-J. and S.C. Dexter, "Effect of Biofilms on Crevice Corrosion of Stainless Steels in Coastal Seawater," *Corrosion*, Vol. 51, No. 1, 1995, pp. 56-66.

113. Martin, F.J., K.E. Lucas, and E.A. Hogan, "Experimental procedure for crevice corrosion studies of Ni–Cr–Mo alloys in natural seawater," *Review of Scientific Instruments*, Vol. 73, No. 3, 2002, pp. 1273-1276.

114. ASTM G71-81(2019), *Standard Guide for Conducting and Evaluating Galvanic Corrosion Tests in Electrolytes.* West Conshohocken, PA; ASTM International, 2019.

115. Salinas-Bravo, V.M. and R.C. Newman, "An alternative method to determine critical pitting temperature of stainless steels in ferric chloride solution," *Corrosion Sci.*, Vol. 36, No. 1, 1994, pp. 67-77.

116. Garfias-Mesias, L.F. and J.M. Sykes, "Effect of copper on active dissolution and pitting corrosion of 25% Cr duplex stainless steels," *Corrosion*, Vol. 54, No. 1, 1998, pp. 40-47.

117. Garfias-Mesias, L.F. and J.M. Sykes, "Metastable pitting in 25 Cr duplex stainless steel," *Corrosion Science*, Vol. 41, No. 5, 1999, pp. 959-987.

118. Garfias-Mesias, L.F., J.M. Sykes, and C.D.S. Tuck, "The effect of phase compositions on the pitting corrosion of 25 Cr duplex stainless steel in chloride solutions," *Corrosion Science*, Vol. 38, No. 8, 1996, pp. 1319-1330.

119. Tsaprailis, T., et al. "Corrosion Resistance of Stainless Steels Exposed to Aggressive Environments with Particles and Water," CORROSION/09, Paper No. 09277, Atlanta, GA: NACE International, 22-26 March 2009.

120. Cottis, R.A., "Interpretation of Electrochemical Noise Data," *Corrosion*, Vol. 57, No. 3, 2001, pp. 265-285.

121. ASTM G199-09, *Standard Guide for Electrochemical Noise Measurement.* West Conshohocken, PA; ASTM International, 2014.

122. ASTM G59-97, *Standard Test Method for Conducting Potentiodynamic Polarization Resistance Measurements.* West Conshohocken, PA; ASTM International, 2014.

123. Wilde, B.E., "A Critical Appraisal of Some Popular Laboratory Electrochemical Tests for Predicting the Localized Corrosion Resistance of Stainless Alloys in Sea Water," *Corrosion*, Vol. 28, No. 8, 1972, pp. 283-291.

124. Wilde, B.E., "Adaptation of Linear Polarization Techniques for in-Situ Corrosion Measurements in Water Cooled Nuclear Reactor Environments," *Corrosion*, Vol. 23, No. 12, 1967, pp. 379-&.

125. Sridhar, N. and G.A. Cragnolino, "Applicability of Repassivation Potential for Long-Term Prediction of Localized Corrosion of Alloy 825 and Type 316L Stainless Steel," *Corrosion*, Vol. 49, No. 11, 1993, pp. 885-894.

126. Park, J.-J., et al., "Effect of Bicarbonate Ion Additives on Pitting Corrosion of Type 316L Stainless Steel in Aqueous 0.5 M Sodium Chloride Solution," *Corrosion*, Vol. 55, No. 4, 1999, pp. 380-387.

127. Aoyama, T., et al., "In situ monitoring of crevice corrosion morphology of Type 316L stainless steel and repassivation behavior induced by sulfate ions," *Corrosion Science*, Vol. 127, 2017, pp. 131-140.

128. Burstein, G.T. and J.J. Moloney, "Cyclic thermammetry," *Electrochemistry Communications*, Vol. 6, No. 10, 2004, pp. 1037-1041.

129. Clerc, C.O., et al., "Assessment of wrought ASTM F1058 cobalt alloy properties for permanent surgical implants," *J Biomed Mater Res*, Vol. 38, No. 3, 1997, pp. 229-34.

130. Rondelli, G., B. Vicentini, and A. Cigada, “Localised corrosion tests on austenitic stainless steels for biomedical applications,” *British Corrosion Journal*, Vol. 32, No. 3, 1997, pp. 193-196.

131. Rondelli, G. and B. Vicentini, “Localized corrosion behaviour in simulated human body fluids of commercial Ni-Ti orthodontic wires,” *Biomaterials*, Vol. 20, No. 8, 1999, pp. 785-92.

132. Tsujikawa, S., “Critical Depth for Initiation of Growing Crevice Corrosion,” *Critical Factors in Localized Corrosion*, G.S. Frankel and R. Newman, Eds., The Electrochemical Society: Pennington, NJ, 1992, pp. 378-388.

133. Tsujikawa, S. and S. Okayama, “Repassivation method to determine critical conditions in terms of electrode potential, temperature and NaCl concentration to predict crevice corrosion resistance of stainless steels,” *Corrosion Science*, Vol. 31, No. 1, 1990, pp. 441-446.

134. ASTM G192, *Determining the Crevice Repassivation Potential of corrosion-resistant alloys using a Potentiodynamic-Galvanostatic-Potentiostatic technique.* West Conshohocken, PA; ASTM International, 2014.

135. Tsujikawa, S. and Y. Hisamatsu, “On the repassivation potential for crevice corrosion,” *Corr. Eng. (Jpn)*, Vol. 29, No. 1, 1980, pp. 37-40.

136. Evans, K.J., et al., “Using Electrochemical Methods to Determine Alloy 22’s Crevice Corrosion Repassivation Potential,” *JOM*, Vol. 57, 2005, pp. 56-61.

137. Mishra, A.K. and G.S. Frankel, “Crevice Corrosion Repassivation of Alloy 22 in Aggressive Environments,” *Corrosion*, Vol. 64, No. 11, 2008, pp. 836-844.

138. Evans, K., et al. “The Use of ASTM G192 (Tsujikawa-Hisamatsu Electrochemical Method) to Evaluate the Susceptibility of Hanford Tank Steels to Pitting Corrosion,” CORROSION 2016, Paper 7688, Houston, TX: NACE International 2016.

139. Rodríguez, M.A., R.M. Carranza, and R.B. Rebak, “Effect of Potential on Crevice Corrosion Kinetics of Alloy 22,” *Corrosion*, Vol. 66, No. 1, 2010, pp. 015007-015007-14.

140. Mishra, A.K. and D.W. Shoesmith, “Effect of Alloying Elements on Crevice Corrosion Inhibition of Nickel-Chromium-Molybdenum-Tungsten Alloys Under Aggressive Conditions: An Electrochemical Study,” *Corrosion*, Vol. 70, No. 7, 2014, pp. 721-730.

141. Hornus, E.C., et al., “Effect of Temperature on the Crevice Corrosion of Nickel Alloys Containing Chromium and Molybdenum,” *Journal of the Electrochemical Society*, Vol. 162, No. 3, 2014, pp. C105-C113.

142. Rincón-Ortíz, M., et al., “Determination of the Crevice Corrosion Stabilization and Repassivation Potentials of a Corrosion-Resistant Alloy,” *Corrosion*, Vol. 66, No. 10, 2010, pp. 105002-105002-12.

143. Okayama, S., S. Tsujikawa, and K. Kikuchi, “The Effect of Alloying Elements on Depassivation pH for Stainless Steels,” *Corrosion Engineering (Jpn.)*, Vol. 36, No. 11, 1987, pp. 702-709.

TABLES

TABLE 1 — Comparison of non-electrochemical test methods to evaluate crevice corrosion resistance.

Method	Summary	
ASTM G48 Method B (rubber band)	Uses	• Pitting & Crevice Resistance in chloride environments. • Rank alloy performance. • Applicable to stainless steels and nickel-base alloys.

	Exposure Conditions	○ Electrolyte: 6 wt% $FeCl_3$ (unadjusted pH approx. 1.0 – 2.0)
		○ Recommended test temperatures:
		  ○ 22 ± 2 °C
		  ○ 50 ± 2 °C
		  ○ Other values could be used.

	Crevice Assembly	• Cylindrical TFE-fluorocarbon blocks. • Fluorinated O-rings or rubber bands (low S).
	Test Duration	○ 72-h (recommended). ○ Variations are allowed, which depend on the alloy composition. ○ Periodic extractions are possible (could lead to variations in the rate of attack).
	Assessment	• Visual inspection (ASTM G46 suggested). • Weight loss to 0.001g or better accuracy.
ASTM G48 Methods D & F	Uses	○ Determine the critical crevice temperature (CCT). ○ Nickel-base and chromium-bearing alloys: Method D. ○ Stainless steels: Method F. ○ It can be used to rank alloy performance.

	Exposure Conditions	• Electrolyte: 6 wt% $FeCl_3$ + 1 wt% HCl (pH adjusted approx. 1.0).
		• Start temperature (nearest 5 °C):
		  ○ Method D: (1.5 × %Cr) + (1.9 × %Mo) + (4.9 × %Nb) + (8.6 × %W) – 36.2.
		  ○ Method F: (3.2 × %Cr) + (7.6 × %Mo) + (10.5 × %N) – 81.0.
		• Minimum Temperature: 0 °C & Maximum recommended temperature: 85 °C.

	Crevice Assembly	○ Multiple-crevice assembly (MCA)
		  ▪ TFE-fluorocarbon segmented washers.
		  ▪ Different materials and geometries are allowed.
		○ Torque
		  ▪ Method D: 0.28 Nm (40 in-oz).
		  ▪ Method F: 1.58 Nm (14 in-lb).

	Test Duration	• Method D: 72-h. • Method F: 24-h.
	Assessment	○ Visual assessment (could follow ASTM G46): Crevice corrosion is present if local attack > 0.025 mm (0.001 in) in depth. ○ Weigh loss.
ASTM G78	Uses	• Determine the crevice corrosion susceptibility in seawater and other chloride environments. • Applicable to iron- and nickel-base alloys. • It can be used to assess the crevice induction time. • It can be used to determine the critical crevice temperature.
	Exposure conditions	○ Seawater, natural waters, and chloride-containing aqueous electrolytes. ○ Temperature: User-defined and maintained within two ± °C.
	Crevice Assembly	• Many different configurations are allowed, e.g., MCA (various geometries and materials), O-rings, gaskets, strips, coatings (for complex geometries).
	Test Specimens	○ Flat, cylindrical, and complex geometries are allowed. ○ Specimens should maintain a constant bodily exposed to shielded area ratio.
	Test Duration	• 30 days (recommended). • Sampling at different time intervals is allowed.

	Assessment	○ Visual assessment:
		  ○ Maximum crevice depth.
		  ○ Affected area.
		  ○ If using MCA, the number of segments showing crevice corrosion.
		○ Weight loss.

TABLE 2 – Comparison of electrochemical test methods with no external polarization to assess crevice corrosion resistance.

Method	Summary
Corrosion Potential Monitoring	• The initiation of pitting and crevice corrosion in stainless steels and nickel-based alloys leads to a sharp decrease in the corrosion potential (E_{Corr}). • E_{Corr} monitoring can be used to determine induction times. • If done as a function of temperature, E_{Corr} monitoring can be used to determine critical temperatures. • Standards such as ASTM G48 and G78 can be modified to include OCP monitoring. E_{Corr} measurements during ASTM G48 testing can provide a better pass/fail criterion than visual inspection alone. • Because it is non-destructive, E_{Corr} measurements provide a means for field monitoring.
Zero resistance amperometry (ZRA) – Remote Crevice Assembly	○ The remote crevice assembly consists of a creviced sample connected to a non-crevice specimen through a zero-resistance ammeter. ○ The ZRA measures galvanic current and couple potential. ○ It simulates a real crevice setting. ○ The initiation of crevice corrosion is associated with a sharp increase in current. ○ ASTM G71 can be used as a guide. ○ There is no agreement on a critical current value to define crevice initiation.
ZRA – Electrochemical Noise	• Similar to the remote crevice assembly except that it uses two creviced coupons. • Electrochemical current noise is recorded and analyzed over time. • The start of the crevice attack leads to an increase in current (it can be positive or negative depending on the specimen where the attack initiates). • ASTM G199 can be used as guidance.

TABLE 3 – Comparison of potentiostatic electrochemical test methods to assess crevice corrosion resistance.

Method	Summary	
Chronoamperometry	• Chronoamperometry consists of measuring current (or current density) as a function of time at a constant applied potential. • It can be performed using creviced or crevice-free specimens. • Chronoamperometry is primarily used to determine induction times. • When performed at different temperatures, it can be used to determine critical temperatures. • It can also be used to determine the critical repassivation temperatures ($T_{R,\ Crev}$) by reducing the temperature after crevice initiation.	
ASTM F746	Uses	○ Assess the pitting or crevice corrosion resistance of metals and alloys for surgical implants. ○ Determine the critical potential, E_{Crit}, to initiate pitting, crevice, or both. ○ Laboratory screening.
	Exposure Conditions	• Electrolyte: Phosphate Buffered Saline (PBS) solution (7.3 < pH < 7.5). • Temperature: 37 ± 1 °C
	Test Specimen	○ Cylindrical coupons: 6.35 mm in diameter and 20 mm in length. ○ Surface preparation: 600-grit SiC paper.
	Crevice assembly	• Tapered PTFE collar (3.18 mm width). • Force-fit to 10mm from the base of the cylinder
	Procedure	○ Step 1: measure the corrosion potential for 1-h, referred to as E_1. ○ Step 2: stimulation ○ The purpose is to initiate localized corrosion. ○ The applied potential, E_{App}, is set to +800 mV_{SCE}. ○ The Duration depends on the current response: ▪ If i instantly > 500 $\mu A \cdot cm^{-2}$ decrease potential to E_1. ▪ If current generally increases, but i < 500 $\mu A \cdot cm^{-2}$, decrease E_{App} to E_1 after 20s. ▪ If after 15 min there is no sharp increase in current, terminate the test. ○ Step 3: repassivation ○ Decrease E_{App} so that $E_{App} = E_1$. ○ If no repassivation, $E_{Crit} = E_1$. ○ If Repassivation occurs: ▪ After stimulation the new $E_{App} = E_1 + 50$ mV. ○ Repeat until no repassivation after stimulation.
	Assessment	• E_{Crit} (pitting or crevice) • Visual examination.
Modified ASTM G150	Uses	• Determine the potential independent pitting (or crevice) temperature. • Predict the conditions resulting in stable crevice propagation. • Applicable to stainless steels from UNS S31600 to S31254; but could be extended to other alloys.
	Exposure Conditions & Procedure	○ Electrolyte: Deaerated, 1M NaCl (unadjusted pH). ○ Temperature: start at 0 °C, ramp at 1 °C/min. ○ Potentiostatic polarization: ○ +700 mV_{SCE} (recommended). ○ Other values are possible. ○ A test at +800 (or+ 600) mV_{SCE} can be performed to determine changes in CPT
	Test Specimen	• Modified to include creviced coupons.
	Assessment	○ CCT (CPT) defined as the temperature at which i > 100 $\mu A \cdot cm^{-2}$ for 60s. ○ Visual confirmation.

TABLE 4 – Comparison of potentiokinetic electrochemical test methods to assess crevice corrosion resistance.

Method	Summary	
Modified ASTM G61	Uses	• Determine the relative susceptibility to localized corrosion (pitting and crevice corrosion). • Determine critical potentials, e.g., E_{Crev} and $E_{R,Crev}$ if using crevice formers. • If done at different temperatures, determine the critical crevice temperature, often referred to as Electrochemical Critical Temperature. • Check one's experimental technique and instrumentation. • Applicable to Iron, nickel, cobalt-base alloys, but it could be used for other passive alloys. • It shall not be used to correlate with the rate of propagation.
	Exposure conditions	○ Electrolyte: deaerated 3.56 wt% NaCl (neutral pH), but other solutions can be used. ○ Temperature: 25 ± 1 °C (recommended), but it can be done at different temperatures.
	Test Specimens	• Modified to include creviced specimens.
	Procedure	○ Step 1: 1-h corrosion potential stabilization. ○ Step 2: potentiokinetic polarization ○ Scan rate: 0.6 V/h (0.168 mV/s). ○ Scan reversal at i = 5 mA·cm^{-2}. ○ Stop test once hysteresis loop closes or once reaching E_{Corr}.
	Assessment	• E_{Crev} and $E_{R,Crev}$ (or E_P & E_{RP} w/o crevice former). • Hysteresis, $\Delta E = E_{Crev} - E_{R,Crev}$. • Visual confirmation.
ASTM G192 Tsujikawa-Hisamatsu Electrochemical [THE] test or PD-GS-PS.	Uses	○ Determine $E_{R,Crev}$ for corrosion-resistant alloys. ○ It is understood that an alloy will not develop crevice corrosion below $E_{R,Crev}$ under the tested conditions (i.e., electrolyte composition, pH, temperature, etc.). ○ It can be modified to determine the crevice repassivation temperature ($T_{R,Crev}$). ○ Applicable to any corrosion-resistant alloy, but developed for UNS N06022.
	Exposure conditions	• Electrolyte: ○ It can be used with any electrolyte. ○ Developed using 1M NaCl (unadjusted pH). • Temperature: ○ 90 °C (UNS N06022). ○ Lower temperatures can be used for less resistant alloys.
	Procedure	○ Step 1 – Potentiodynamic polarization: ○ 0.6V/h (0.168 mV/s). ○ Until a preset current is reached (2 µA·cm^{-2} for UNS N06022) ○ Step 2 – Galvanostatic period ○ The preset current is kept constant for 2-h. ○ E vs. t is recorded. ○ The goal is to develop & grow crevice attack (if any develops). ○ Step 3 – Potentiostatic polarization ○ The potential is decreased by 10 mV internals. ○ The duration of each step is 2-h ○ I vs. t is recorded at each step. ○ $E_{R,Crev}$ is defined as the highest potential for which the current does not increase as a function of time.
	Assessment	• $E_{R,Crev}$ and visual confirmation.
PD-GS-PD technique	○ The PD-GS-PD technique is a simplification of the THE test. ○ Step 3 is replaced by a potentiodynamic polarization step. ○ $E_{R,Crev}$ is defined as a cross-over potential. ○ It can be used to determine $T_{R,Crev}$.	

TABLE 5–Results of the second interlaboratory test program.

Note 1—Minimum temperature (°C) to produce an attack at least 0.025-mm (0.001-in.) deep on the bold surface of the specimen. Edge attack ignored.

Alloy/Laboratory	Method E—CPT Critical Pitting Corrosion Temperature (°C)				Method F—CCT Critical Crevice Corrosion Temperature (°C)			
	UNS S31603	UNS S31803	UNS S44735	UNS N08367	UNS S31603	UNS S31803	UNS S44735	UNS N08367
1	15/15/[A]	30/30/30	85/85/85	75/[A]	0/0/0	15/[A]/[A]	30/[A]/[A]	30/30/30
2	10/[A]/[A]	25/25/[A]	80/80/80	75/75	0/0/0	15/15/15	30/30/30	25/25/25
3	0/0/0	25/25/[A]	80/80/80	70/70/[A]	0/0/0	20/20/20	35/35/35	30/30/[A]
4	15/15/[A]	30/30/30	75/[A]/[A]	75/75/[A]	0/0/0	20/20/20		20/20/20
5	15/15/15	20/[A]	80/80/80	70/70/70	0/0/0	20/20/20	35/35/35	30/30/30
6		40		75	0/0/0	15	35	25
7	15/15/15	35/35/35	>85/>85/>85	75/75/75	0/0/0	25/25/25	35/[A]/[A]	30/30/30

[A] Test run but no attack observed.

FIGURES

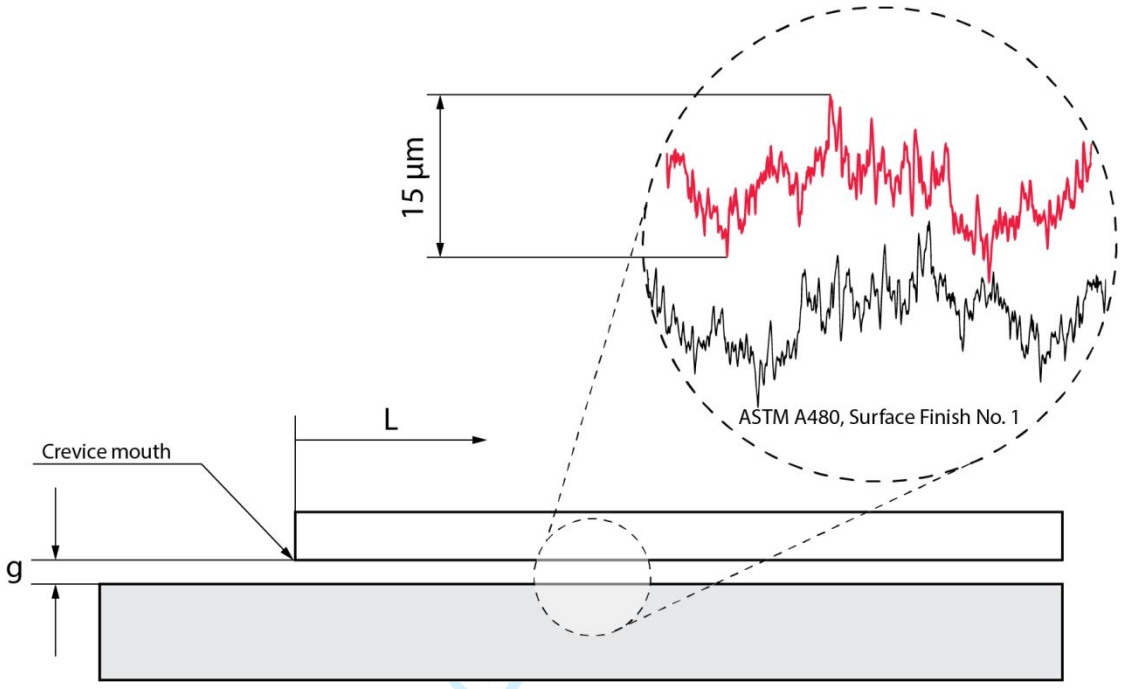

FIG. 1—Geometry of crevice corrosion. In the sketch, the horizontal scale is arbitrary.

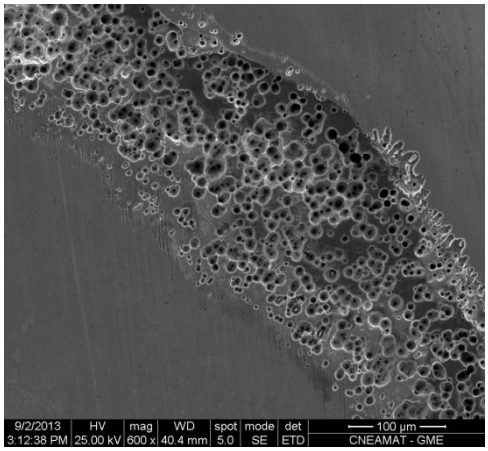

a

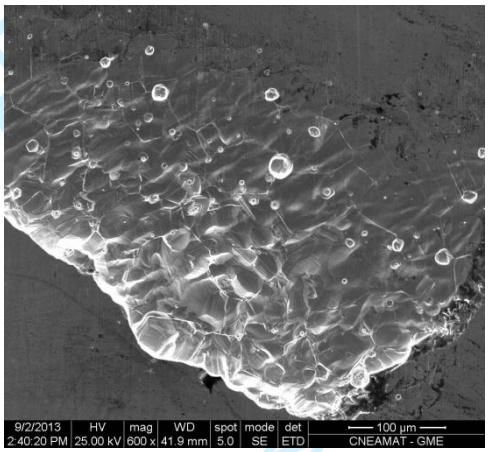

b

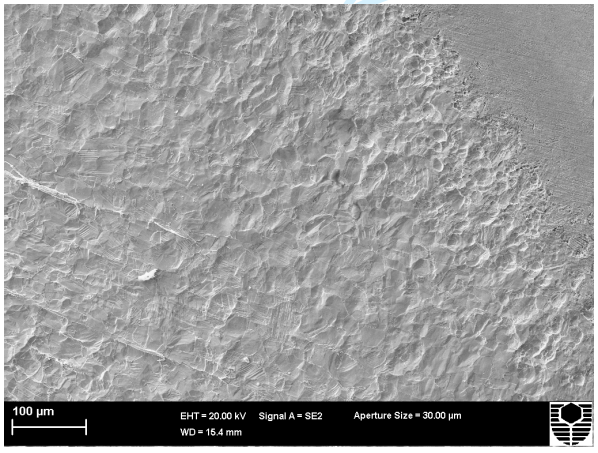

c

FIG. 2—Different crevice attack morphologies (a) pitting corrosion inside the crevice gap on UNS S30403 in 0.1M NaCl at 60 °C, (b) pitting and general dissolution with the crevice gap on UNS S31600 in 0.1M NaCl at 30 °C, and (c) uniform crevice attack on UNS S31603 in 6 wt% $FeCl_3$ at 20 °C.

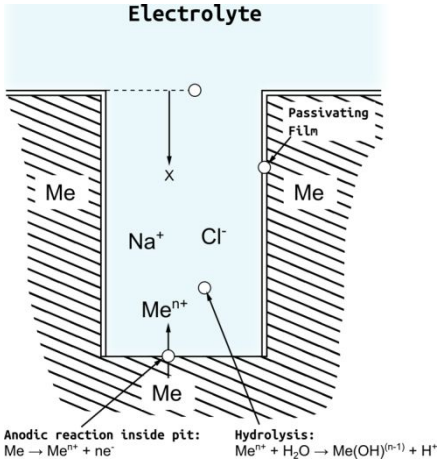

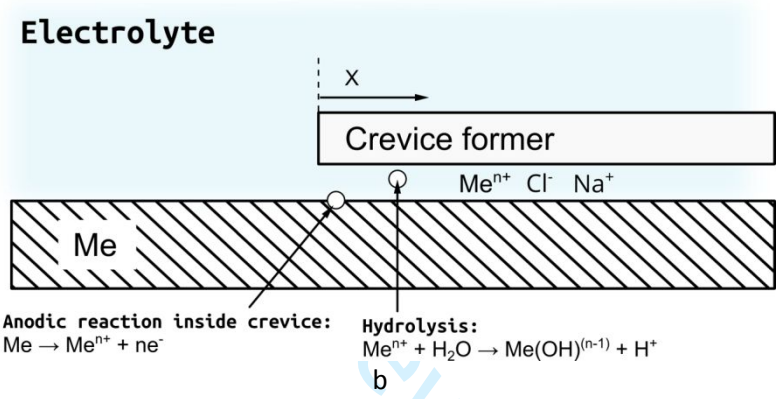

FIG. 3. Unidirectional pit (a) and crevice (b) model.

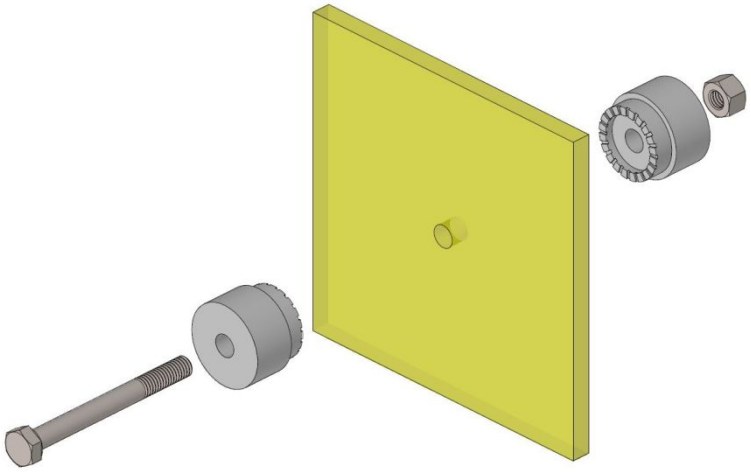

a

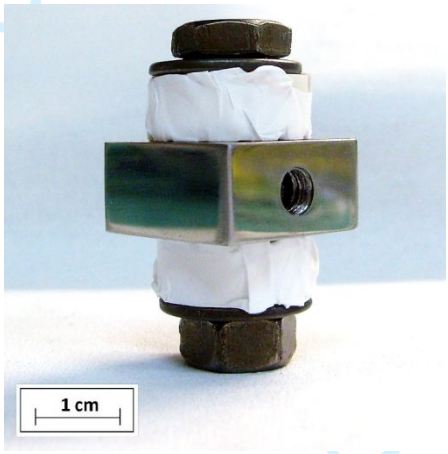

b

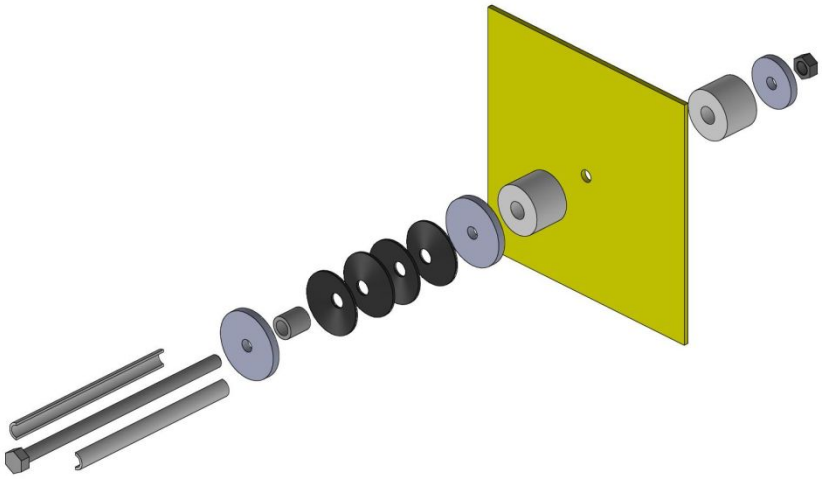

c

FIG. 4 – Different types of MCAs (a) serrated MCA and Ti Gr. 2 bolts and nuts compliant with ASTM G48, (b) assembled PTFE tape-covered ceramic MCA, and (c) a CREVCORR DSMCA setup.

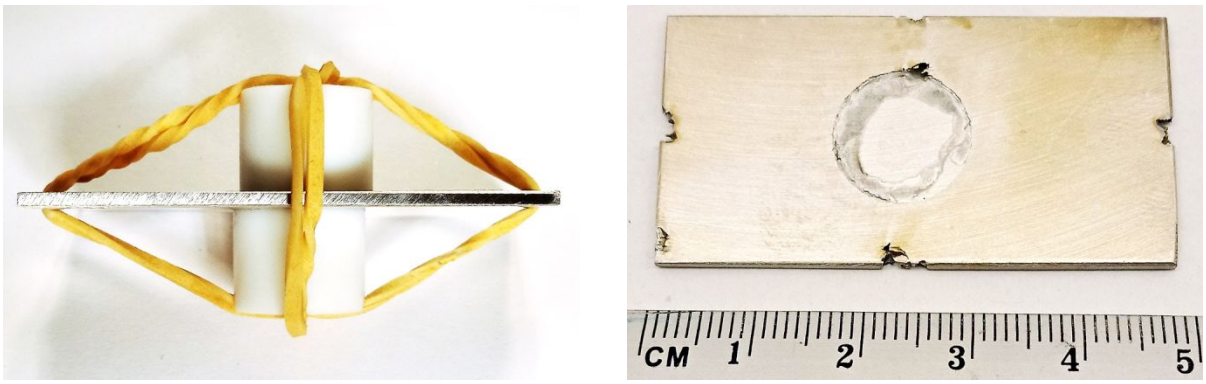

a b

FIG. 5 – ASTM G48 Method B (a) type 304 stainless steel creviced specimen before exposure and (b) crevice corrosion attack after immersion in 6 wt% $FeCl_3$.

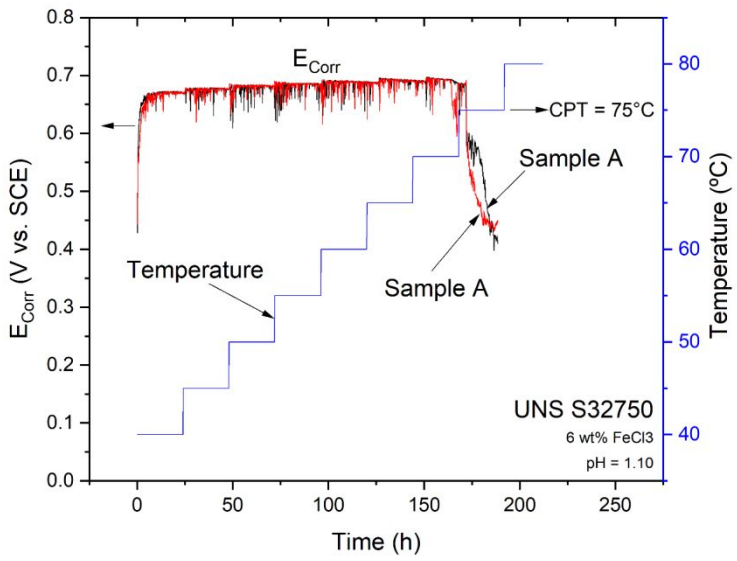

FIG. 6 – E_{Corr} of UNS S32750 as a function of time during immersion in 6 wt% $FeCl_3$ (pH = 1.0) and a stepwise increase in temperature. The duration of each step was 24-h. The sudden drop in E_{Corr} marks the initiation of localized corrosion.

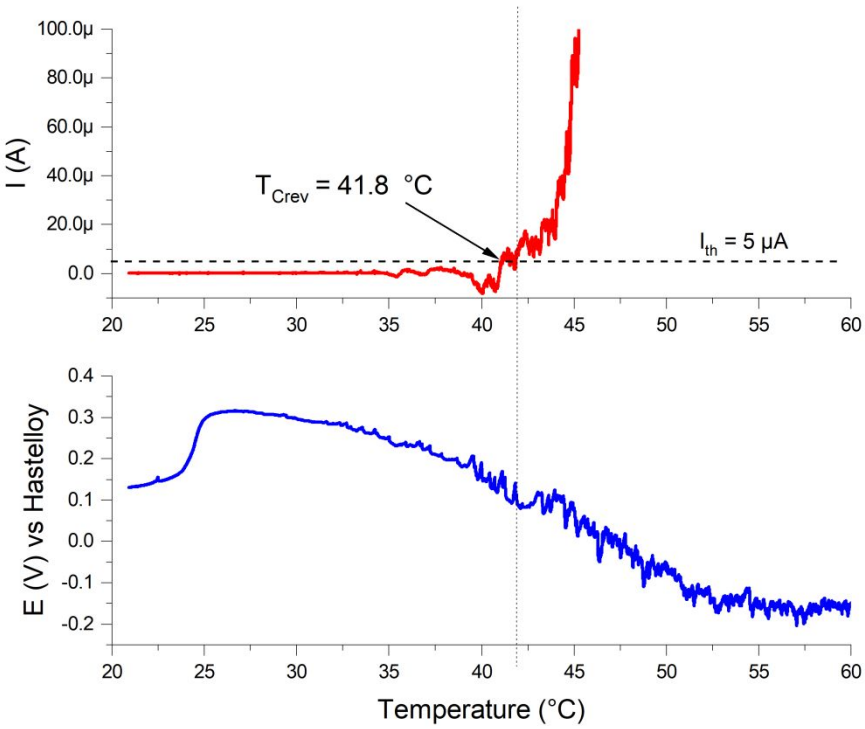

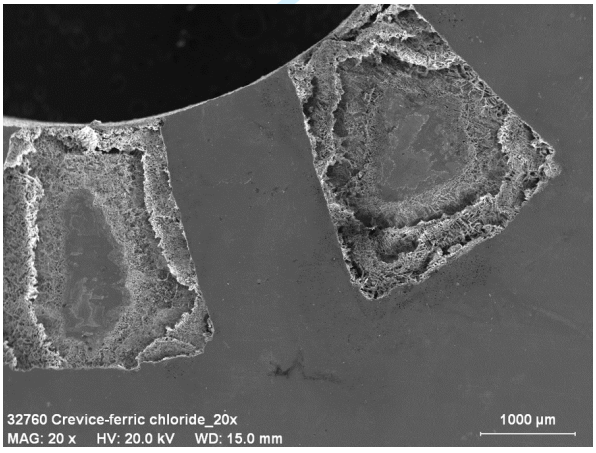

FIG. 7 – ZRA testing of UNS S32760 in 6 wt% $FeCl_3$ (pH = 1.0) (a) current and potential as a function of temperature and (b) crevice corrosion attack.

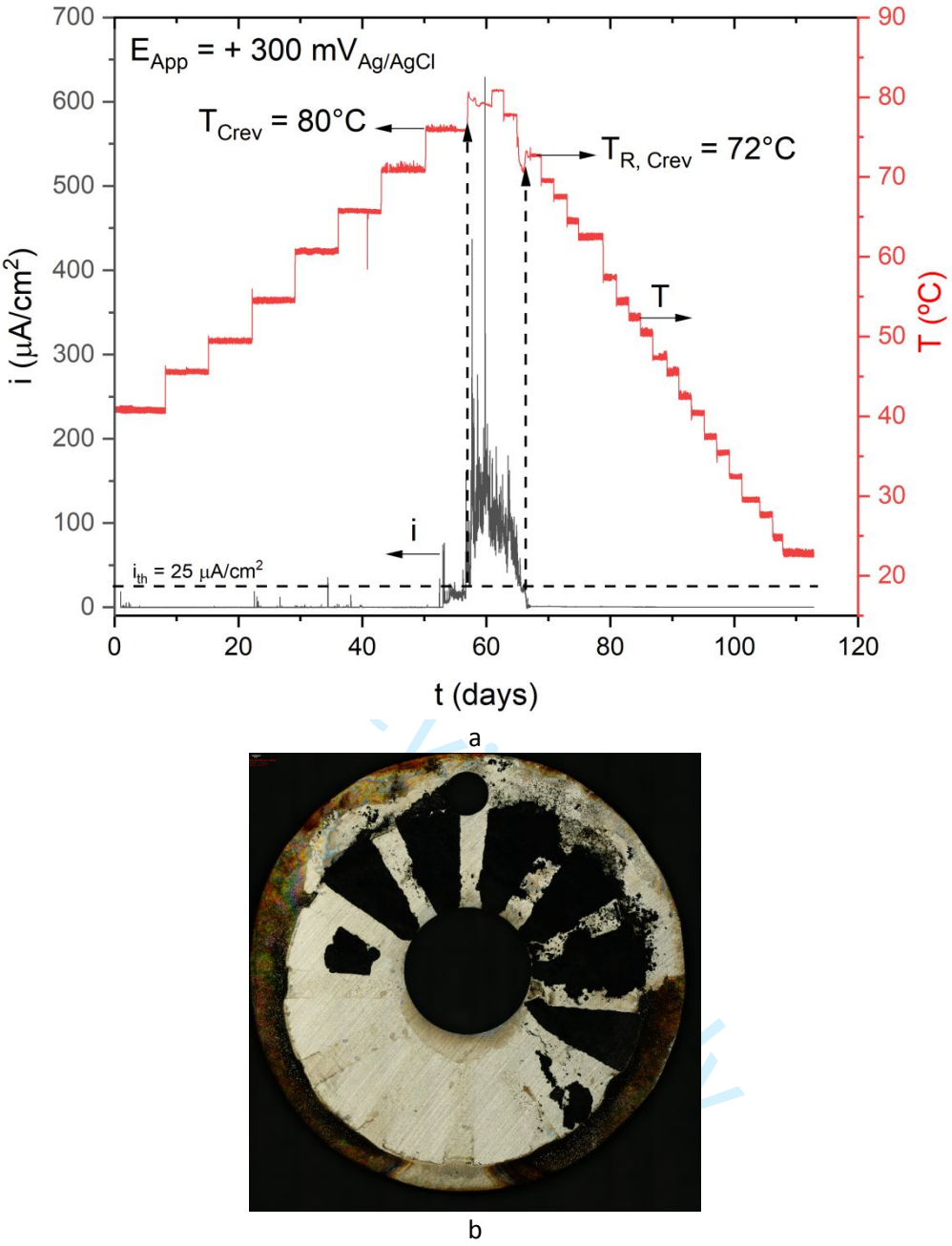

FIG. 8 – (a) Current density and temperature as a function of immersion time of UNS S39274 in natural seawater at an applied potential of E_{App} = +300 mV_{SSE} and (b) visual appearance after 110 days of exposure.

(a)

(b)

FIG. 9 — ASTM F746 crevice assembly (a) exploded view and (b) assembled working electrode.

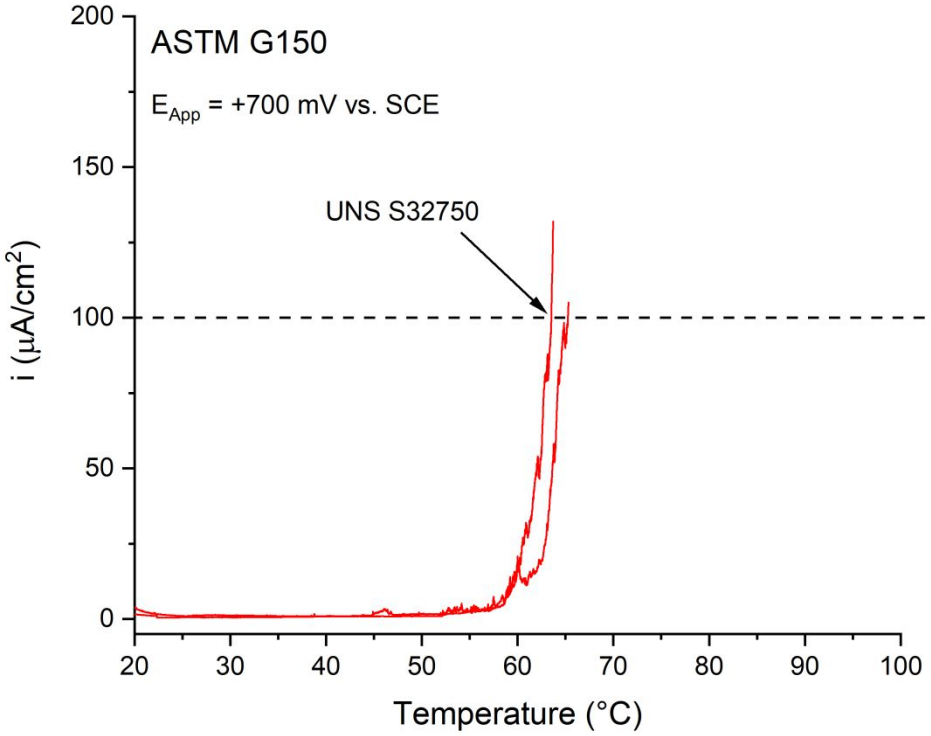

FIG. 10 — An example of i vs. temperature curve of UNS S32750 in 1M NaCl as per ASTM G150.

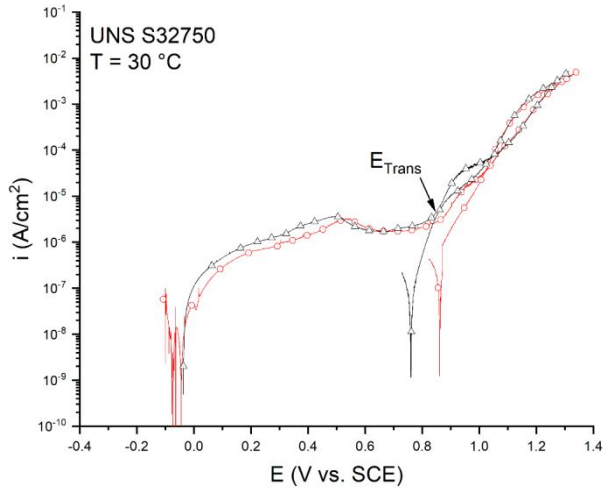

a

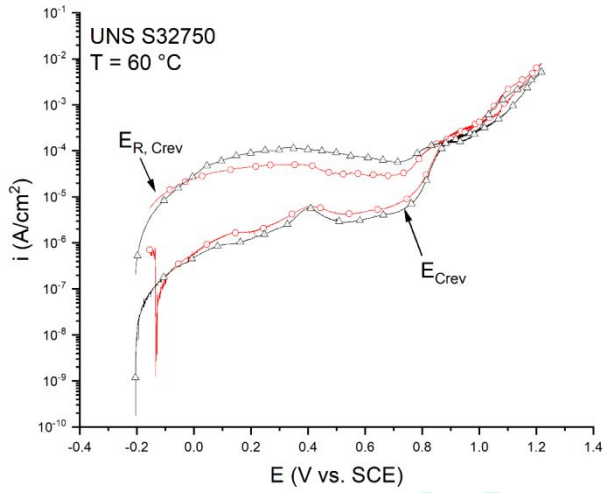

b

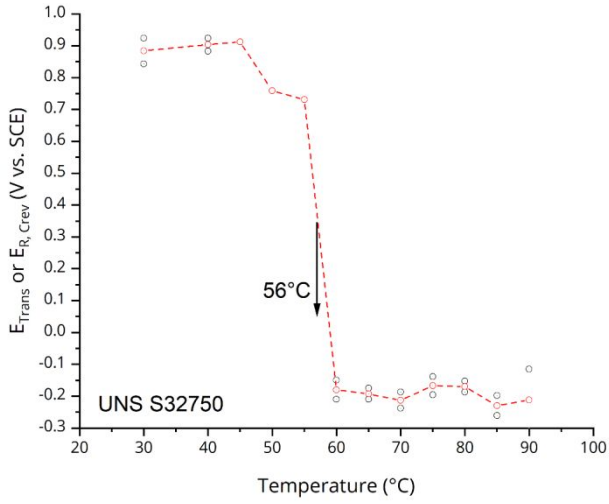

c

FIG. 11 – Cyclic anodic polarizations of creviced UNS S32750 samples in 3.56 wt% NaCl at (a) 30 °C and (b) 60 °C. The critical crevice repassivation temperature is shown in the E vs. T diagram in (C).

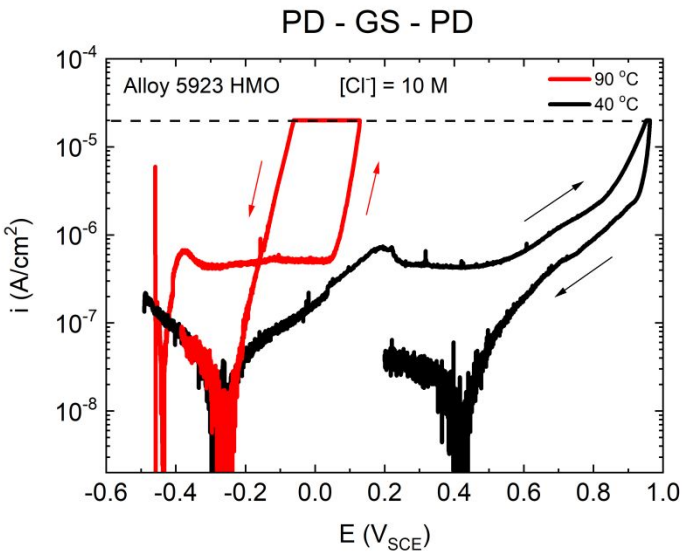

a

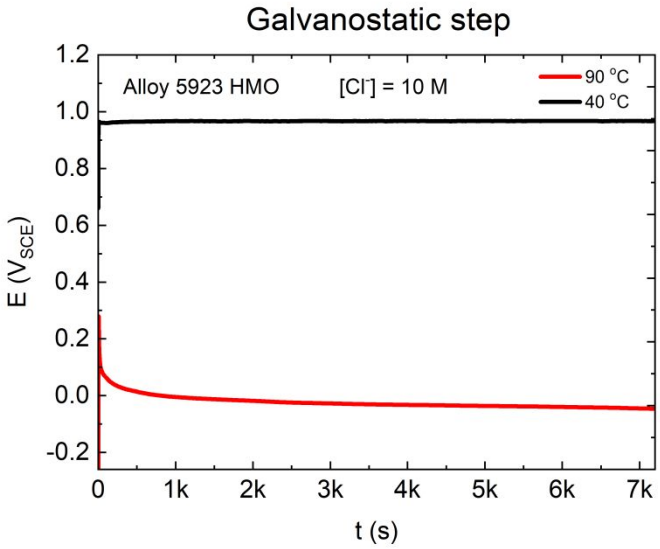

b

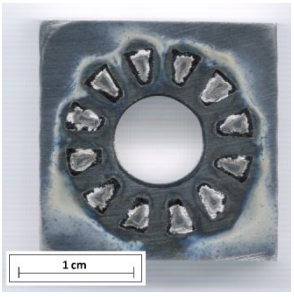

c

FIG. 12 – PD-GS-PD test of UNS N06059 in 10 M Cl^- solution at 40 and 90 °C (a) E vs. I curve, (b) potential vs. time during the GS step, and (c) crevice corrosion attack after testing at 90 °C.

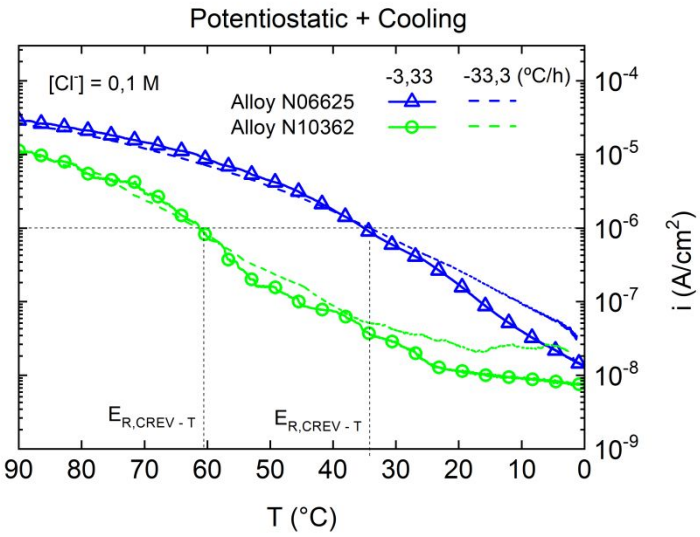

b

FIG. 13 – PD-GS-PD-(PS + Cooling) Step 5 applied to UNS N06625 and N10362 applied potential and cooling rates as indicated.

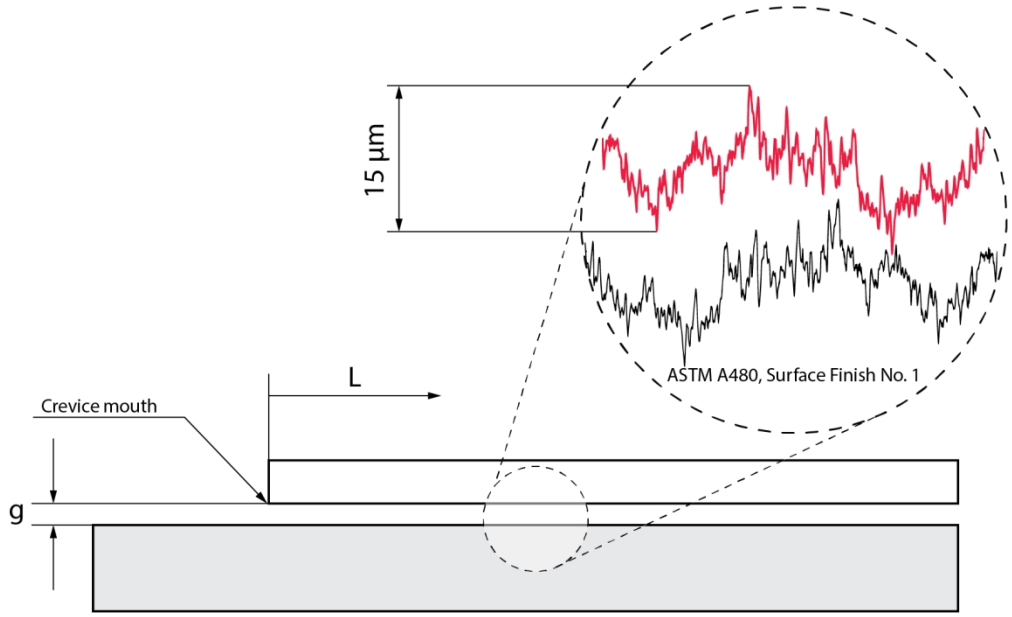

FIG 1

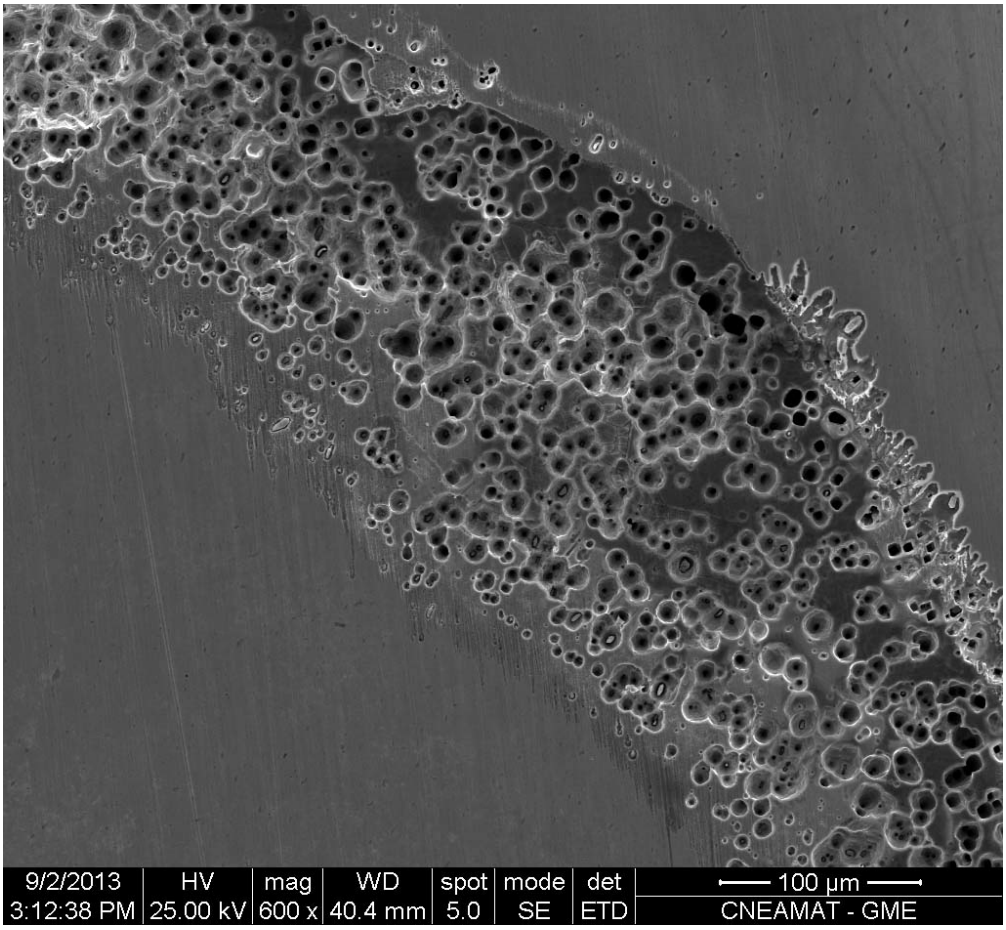

FIG 2a

361x332mm (72 x 72 DPI)

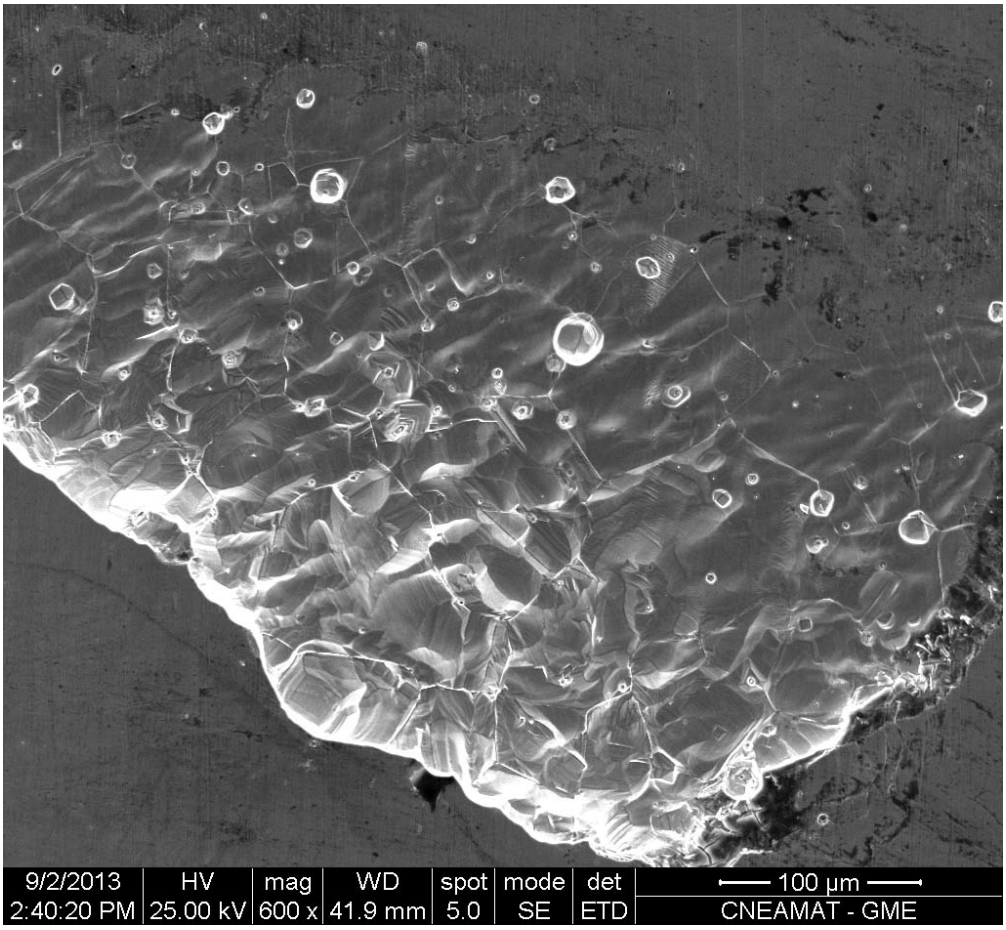

Fig 2b

361x332mm (72 x 72 DPI)

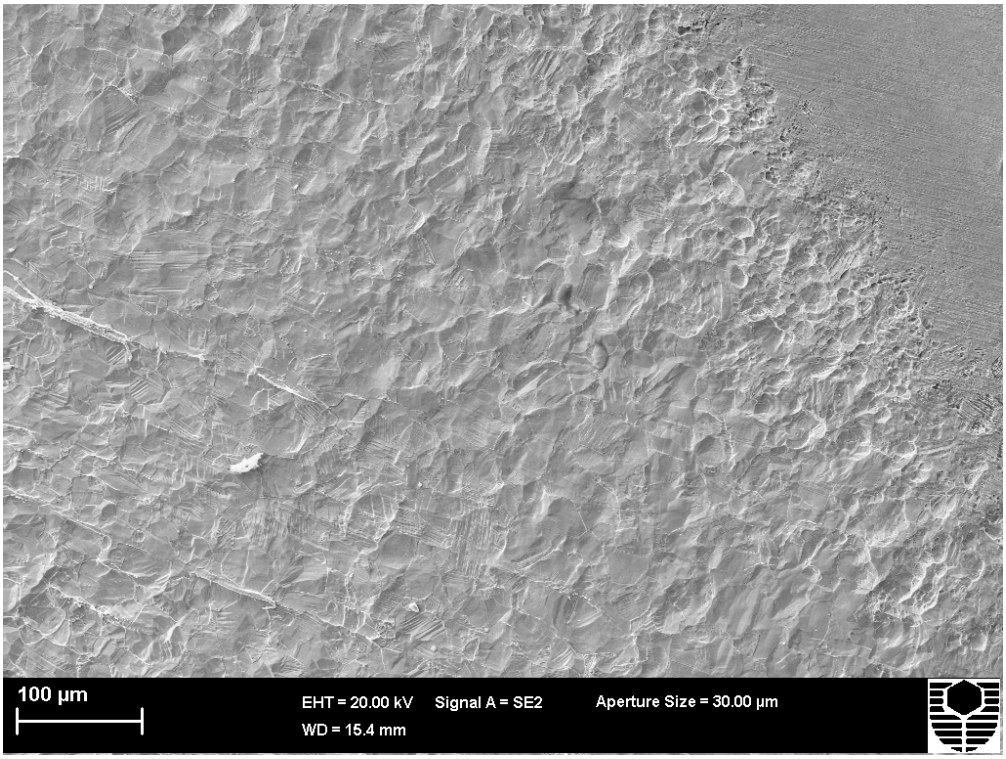

Fig 2c

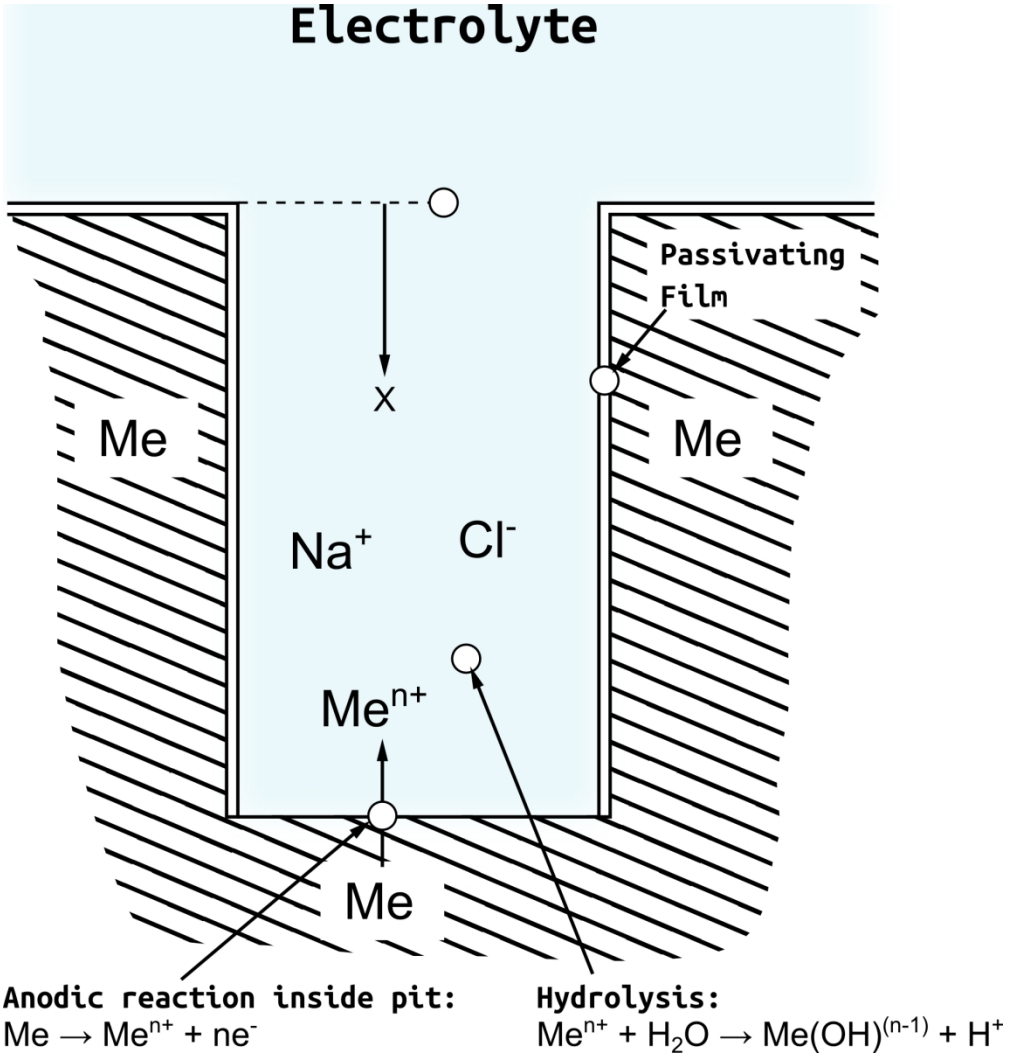
Electrolyte
Passivating Film
X
Me
Me
Na^+
Cl^-
Me^{n+}
Me
Anodic reaction inside pit:
$Me \rightarrow Me^{n+} + ne^-$
Hydrolysis:
$Me^{n+} + H_2O \rightarrow Me(OH)^{(n-1)} + H^+$

Fig 3a

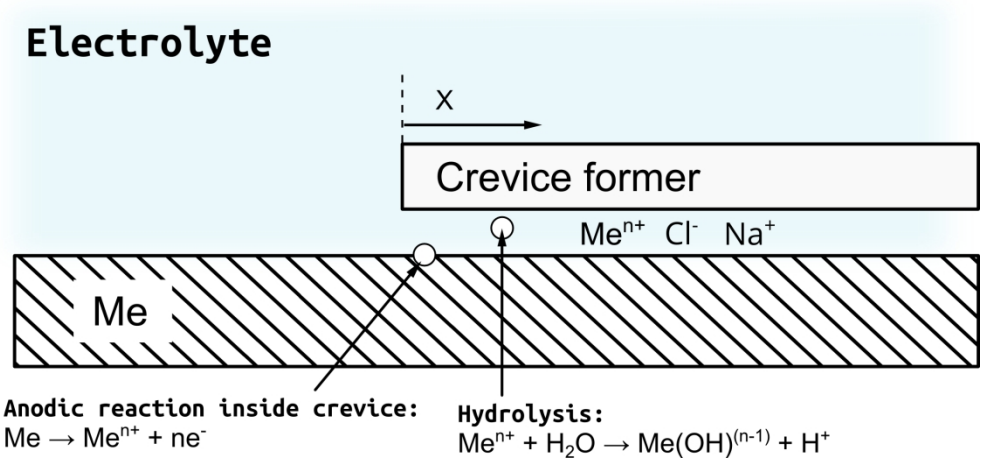
Electrolyte
X
Crevice former
Me^{n+} Cl^- Na^+
Me
Anodic reaction inside crevice:
$Me \rightarrow Me^{n+} + ne^-$
Hydrolysis:
$Me^{n+} + H_2O \rightarrow Me(OH)^{(n-1)} + H^+$

Fig 3b

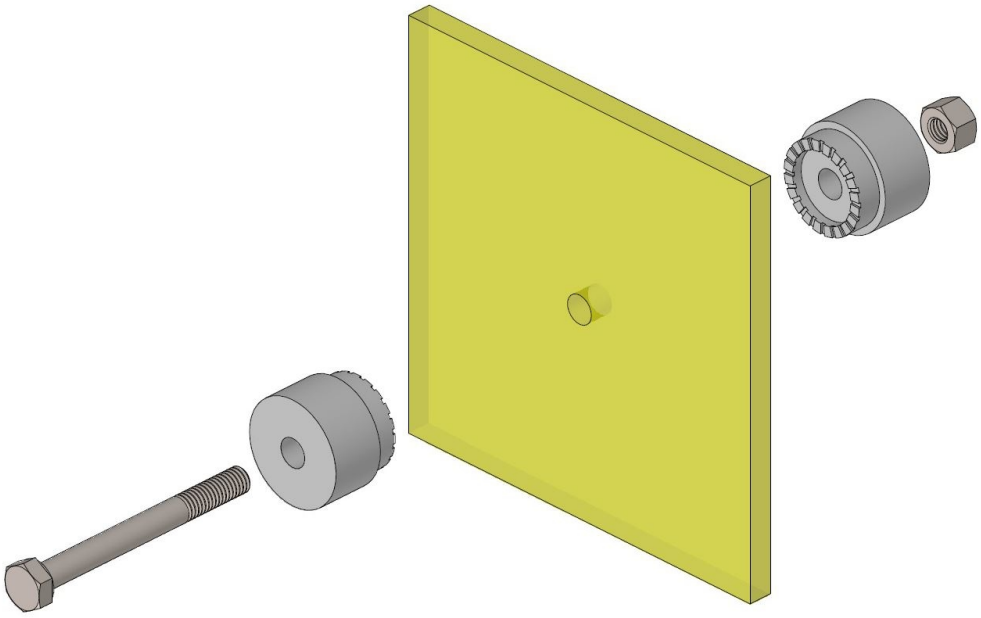

Fig 4a

338x213mm (96 x 96 DPI)

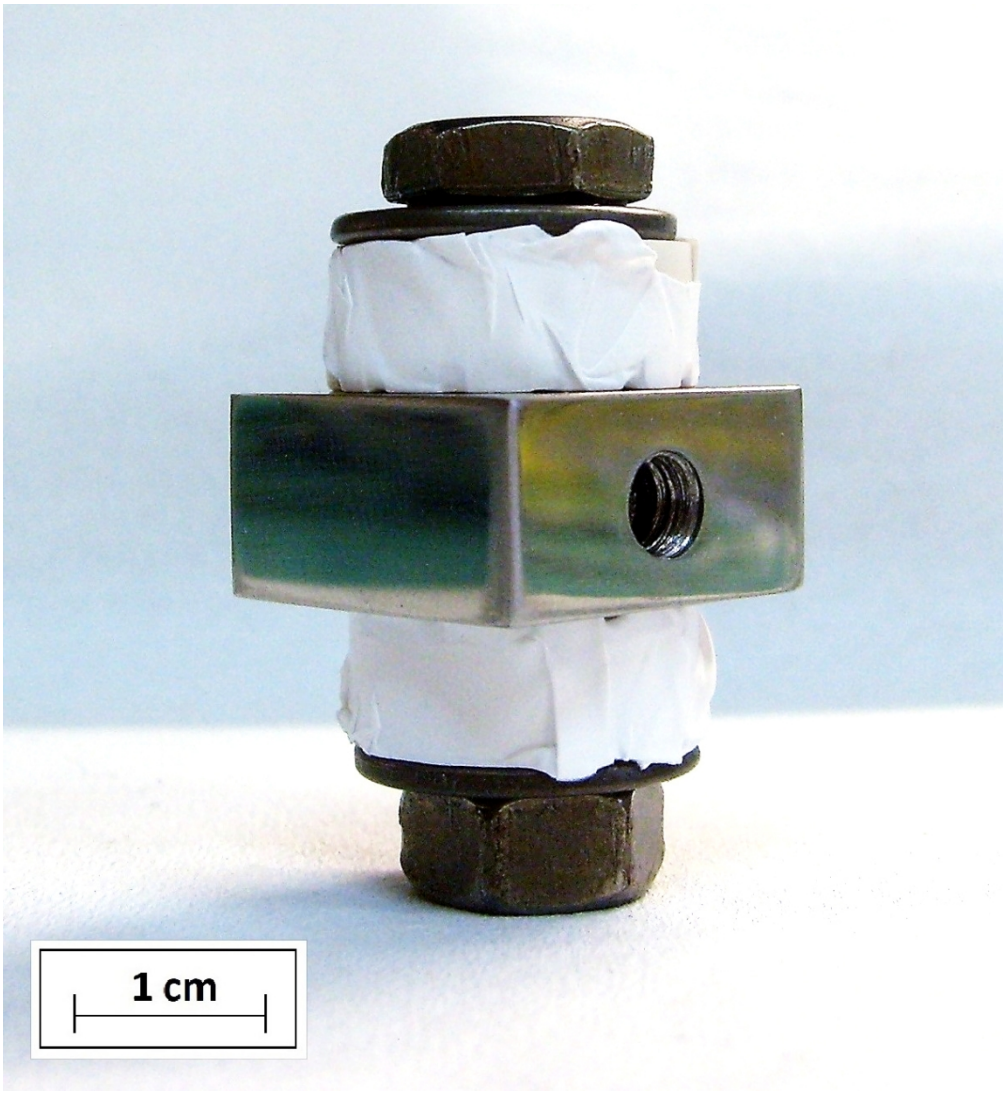

Fig 4b

319x347mm (96 x 96 DPI)

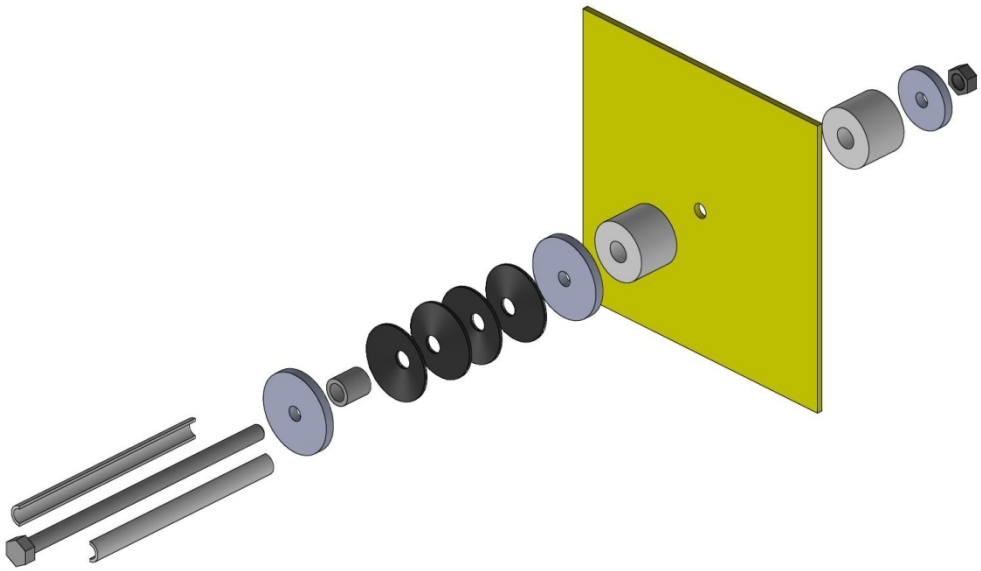

Fig 4c

407x234mm (96 x 96 DPI)

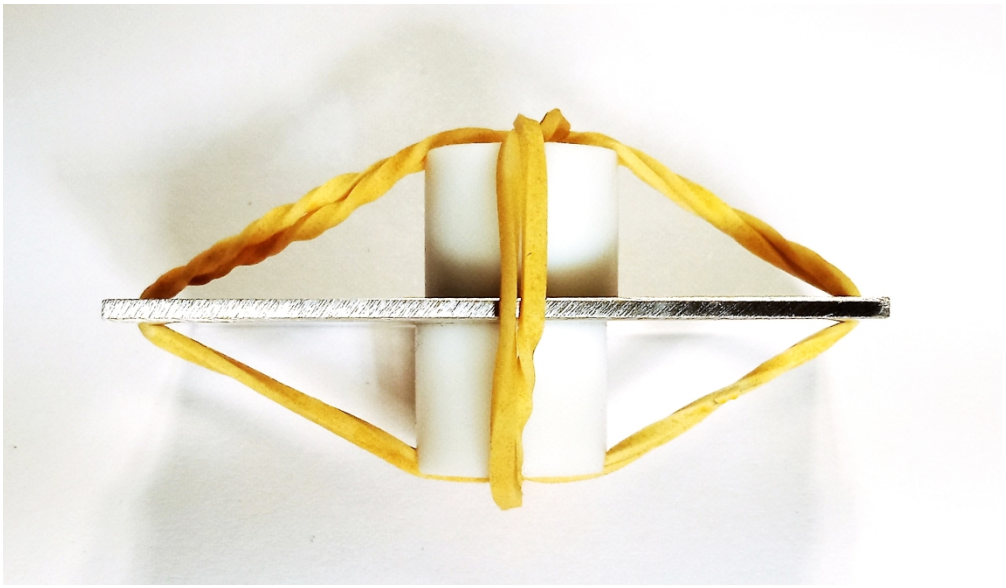

Fig 5a

720x417mm (72 x 72 DPI)

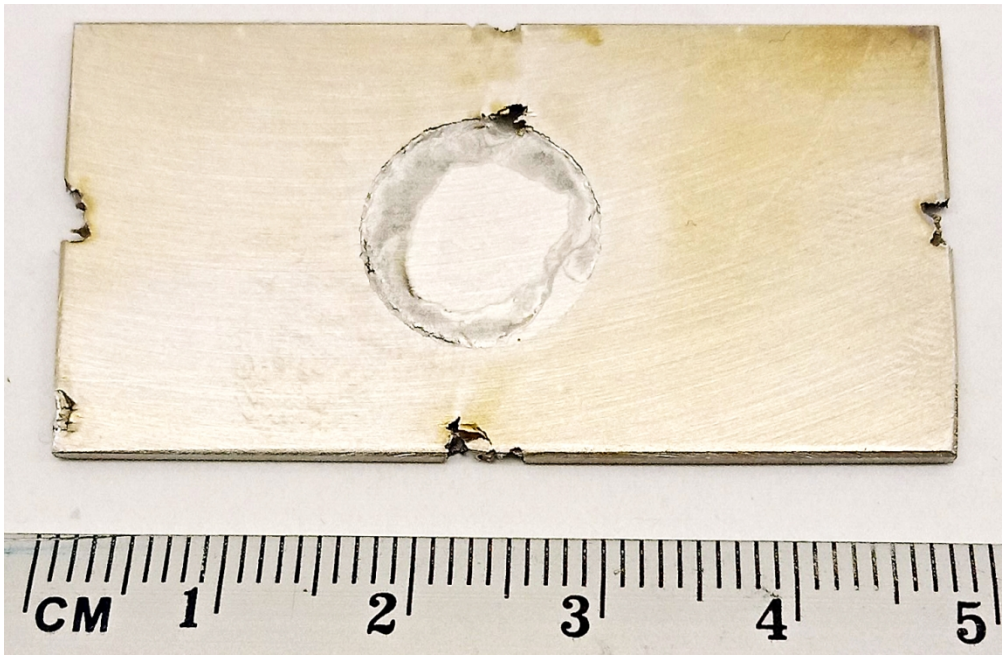

Fig 5b

519x337mm (72 x 72 DPI)

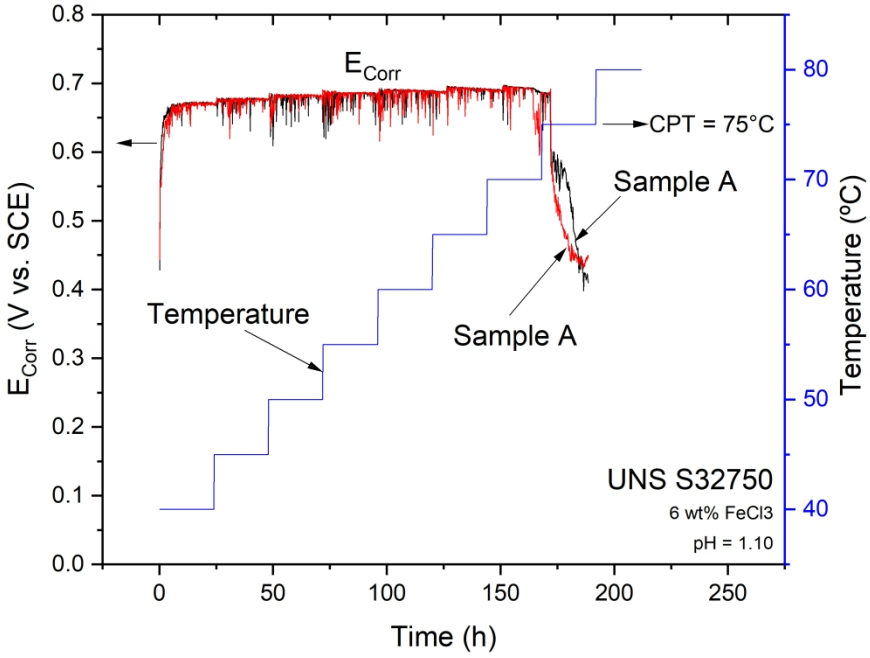
E_Corr
CPT = 75°C
Sample A
Temperature
Sample A
UNS S32750
6 wt% FeCl3
pH = 1.10
E_Corr (V vs. SCE)
Temperature (°C)
Time (h)
0.0
0.1
0.2
0.3
0.4
0.5
0.6
0.7
0.8
40
50
60
70
80
0
50
100
150
200
250

Fig 6

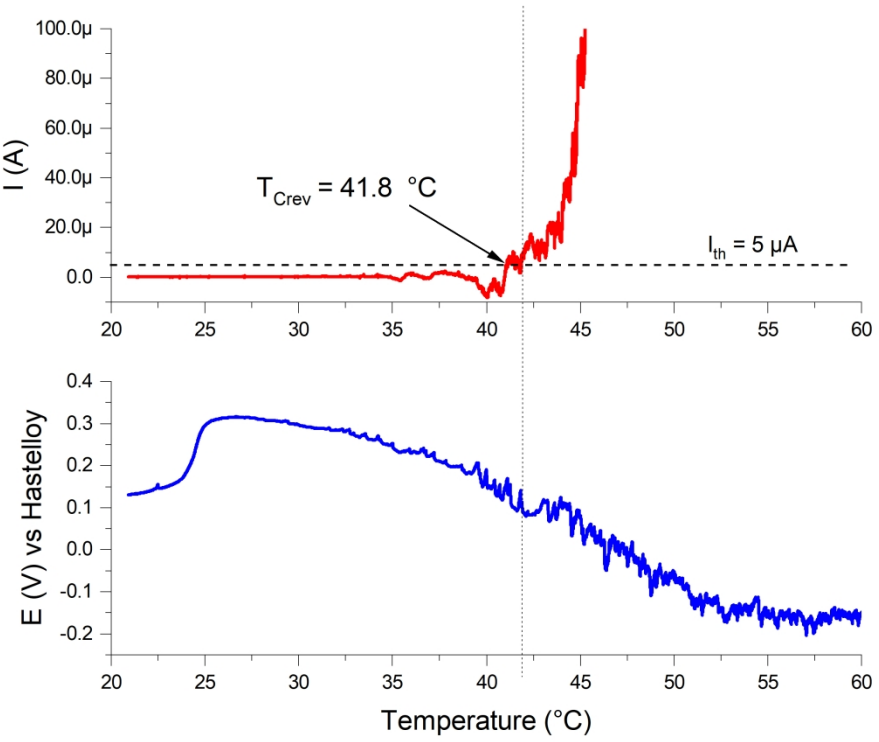
100.0µ
80.0µ
60.0µ
40.0µ
20.0µ
0.0
I (A)
T_{Crev} = 41.8 °C
I_{th} = 5 µA
0.4
0.3
0.2
0.1
0.0
-0.1
-0.2
E (V) vs Hastelloy
20
25
30
35
40
45
50
55
60
Temperature (°C)

Fig 7a

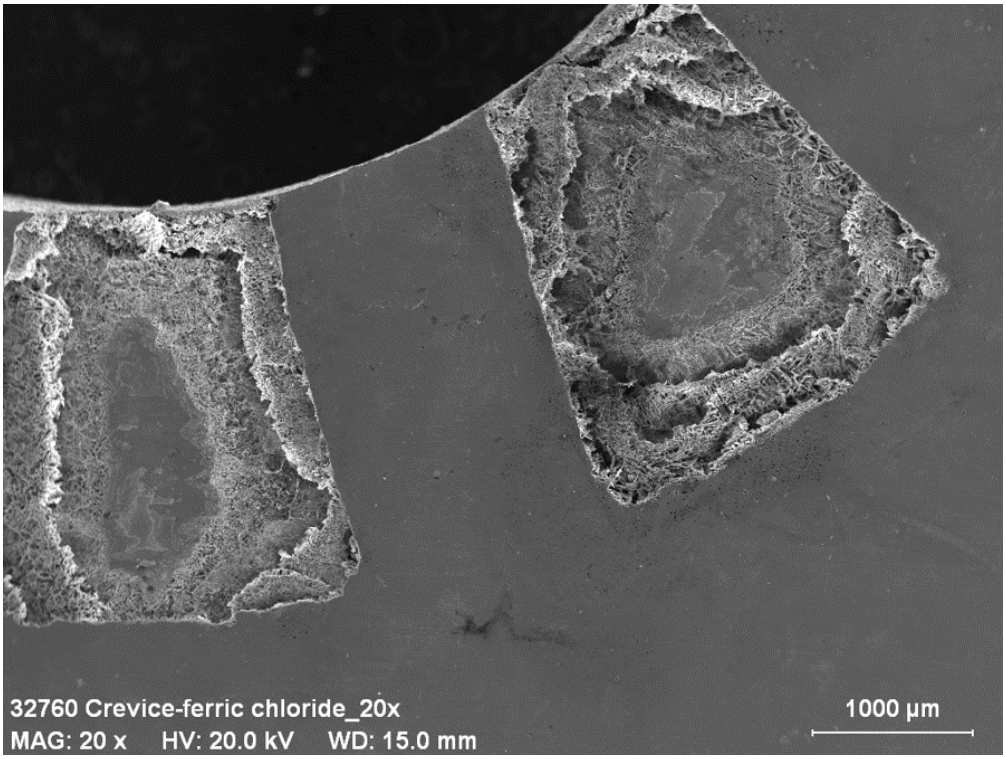
32760 Crevice-ferric chloride_20x
MAG: 20 x HV: 20.0 kV WD: 15.0 mm
1000 µm

Fig 7b

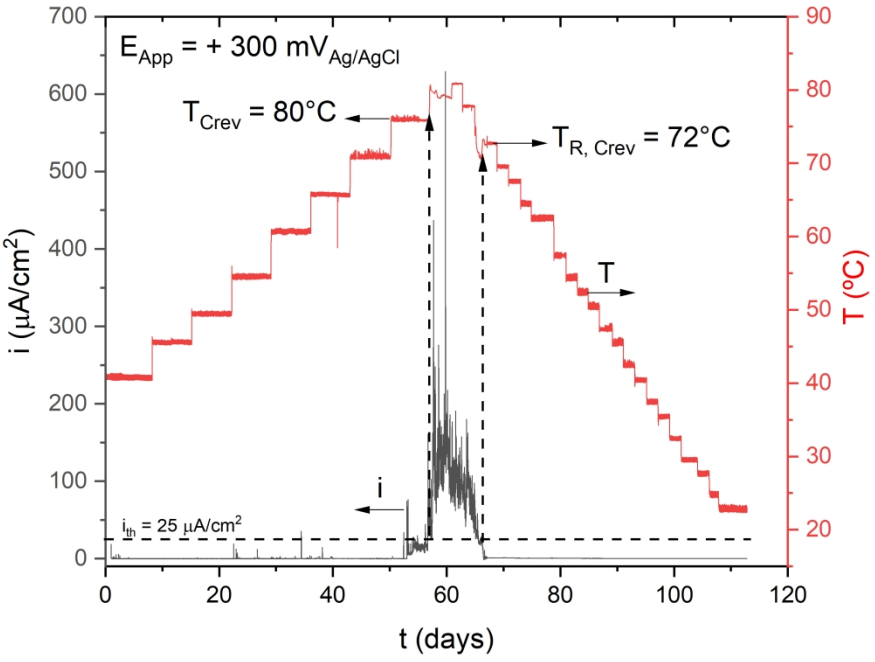
E_App = + 300 mV_Ag/AgCl
T_Crev = 80°C
T_R, Crev = 72°C
T
i
i_th = 25 µA/cm²
i (µA/cm²)
T (°C)
t (days)
0
100
200
300
400
500
600
700
20
30
40
50
60
70
80
90
0
20
40
60
80
100
120

Fig 8a

Fig 8b

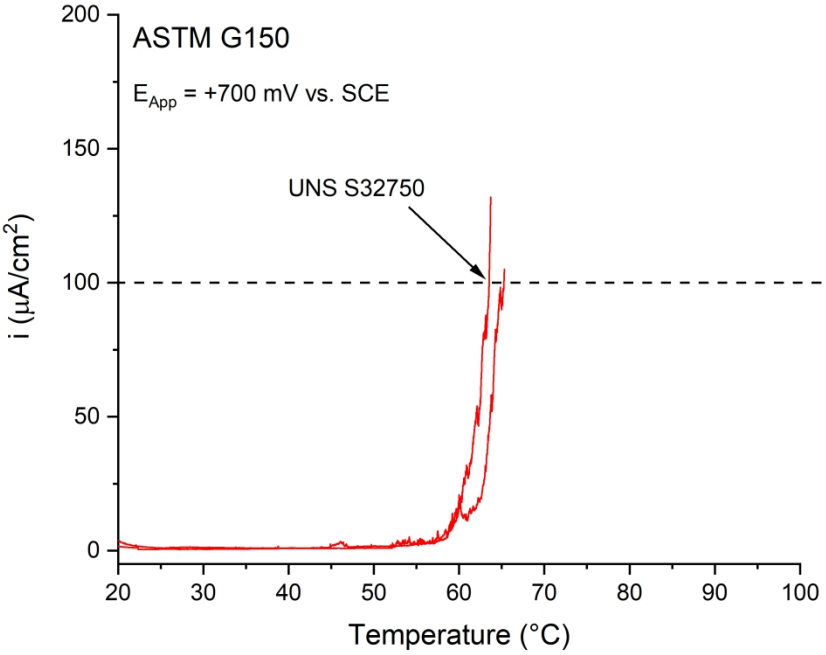
ASTM G150
E_{App} = +700 mV vs. SCE
UNS S32750
i (μA/cm²)
Temperature (°C)
200
150
100
50
0
20
30
40
50
60
70
80
90
100

Fig 10

FIG. 9 — ASTM F746 crevice assembly (a) exploded view and (b) assembled working electrode.

FIG. 9 — ASTM F746 crevice assembly (a) exploded view and (b) assembled working electrode.

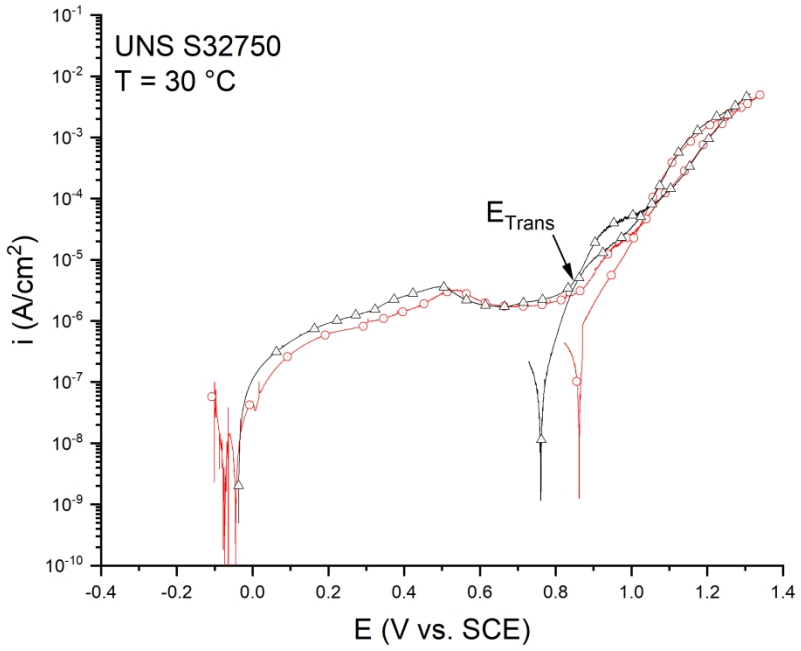
UNS S32750
T = 30 °C
E_Trans
i (A/cm²)
E (V vs. SCE)
10⁻¹
10⁻²
10⁻³
10⁻⁴
10⁻⁵
10⁻⁶
10⁻⁷
10⁻⁸
10⁻⁹
10⁻¹⁰
-0.4
-0.2
0.0
0.2
0.4
0.6
0.8
1.0
1.2
1.4

Fig 11a

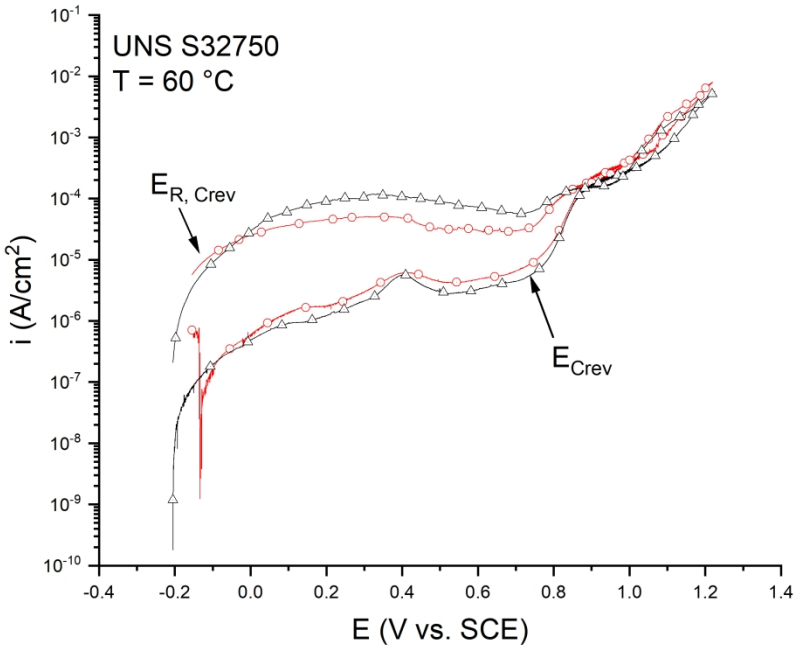

Fig 11b

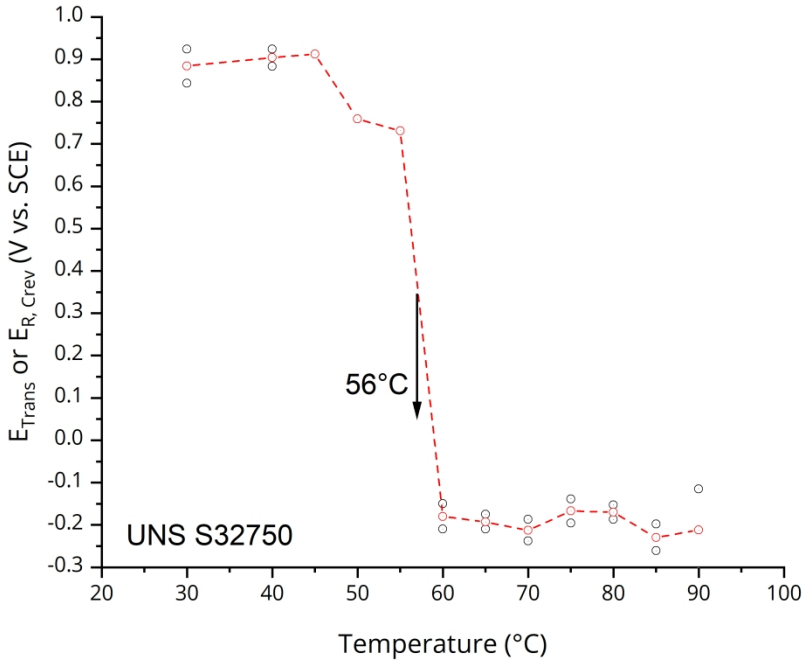
1.0
0.9
0.8
0.7
0.6
0.5
0.4
0.3
0.2
0.1
0.0
-0.1
-0.2
-0.3
E_{Trans} or $E_{R, Crev}$ (V vs. SCE)
56°C
UNS S32750
20
30
40
50
60
70
80
90
100
Temperature (°C)

Fig 11c

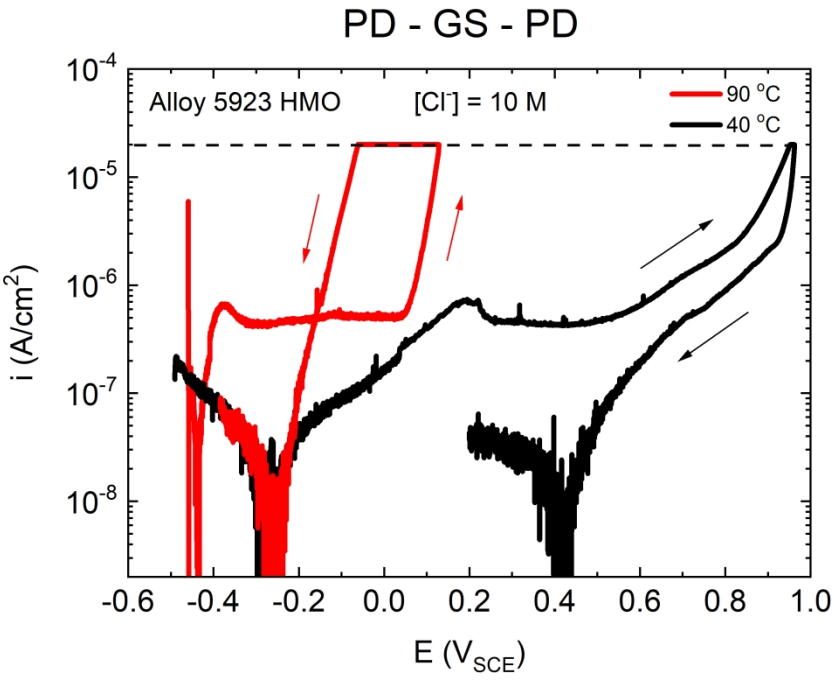
PD - GS - PD
Alloy 5923 HMO
[Cl-] = 10 M
90 °C
40 °C
i (A/cm2)
10-4
10-5
10-6
10-7
10-8
-0.6
-0.4
-0.2
0.0
0.2
0.4
0.6
0.8
1.0
E (VSCE)

Fig 12a

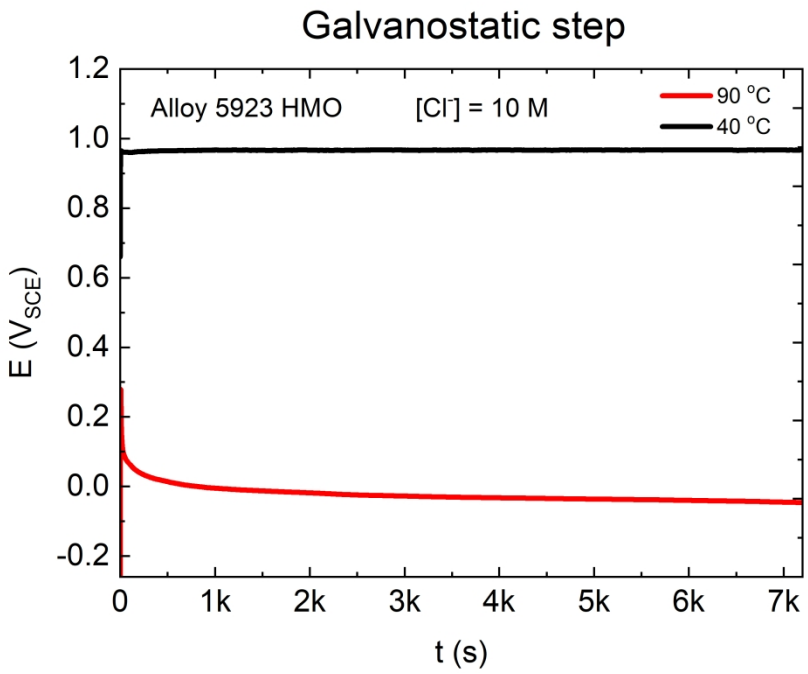
Galvanostatic step
Alloy 5923 HMO
[Cl⁻] = 10 M
90 °C
40 °C
E (V_SCE)
1.2
1.0
0.8
0.6
0.4
0.2
0.0
-0.2
0
1k
2k
3k
4k
5k
6k
7k
t (s)

Fig 12b

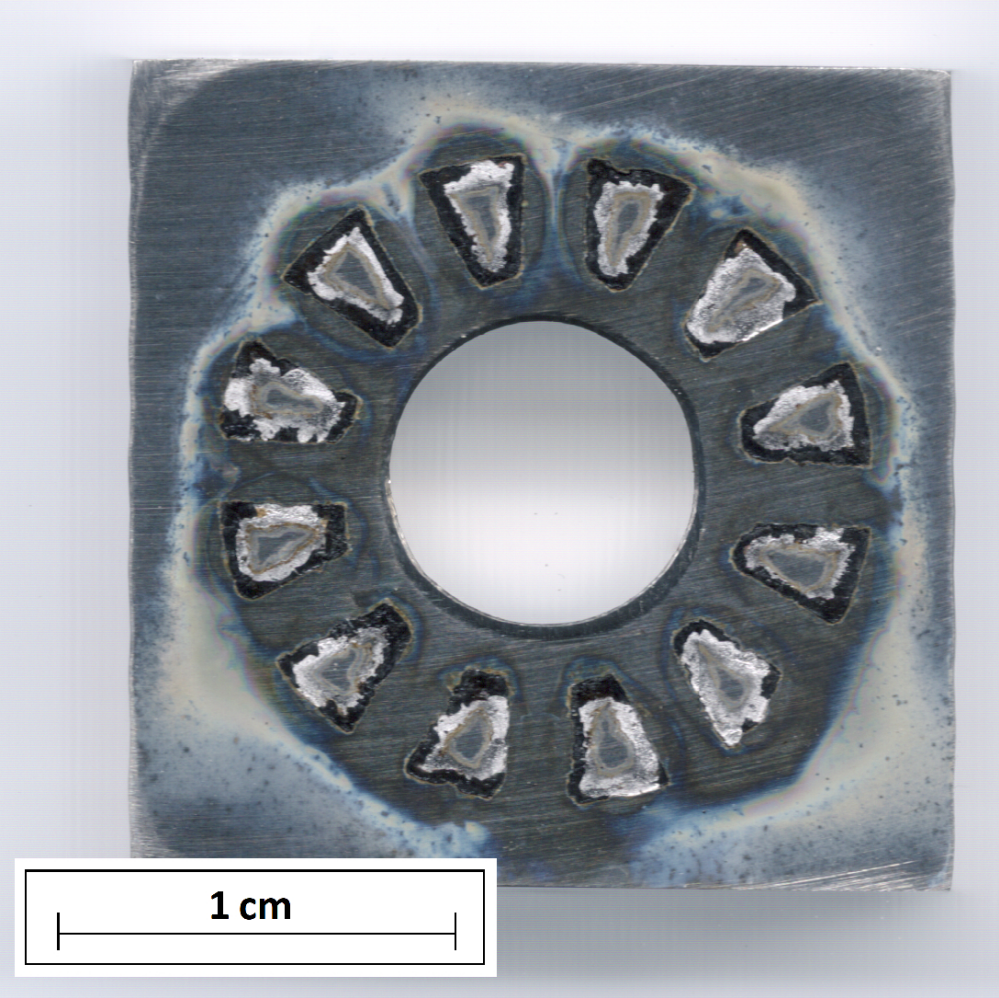

Fig 12c

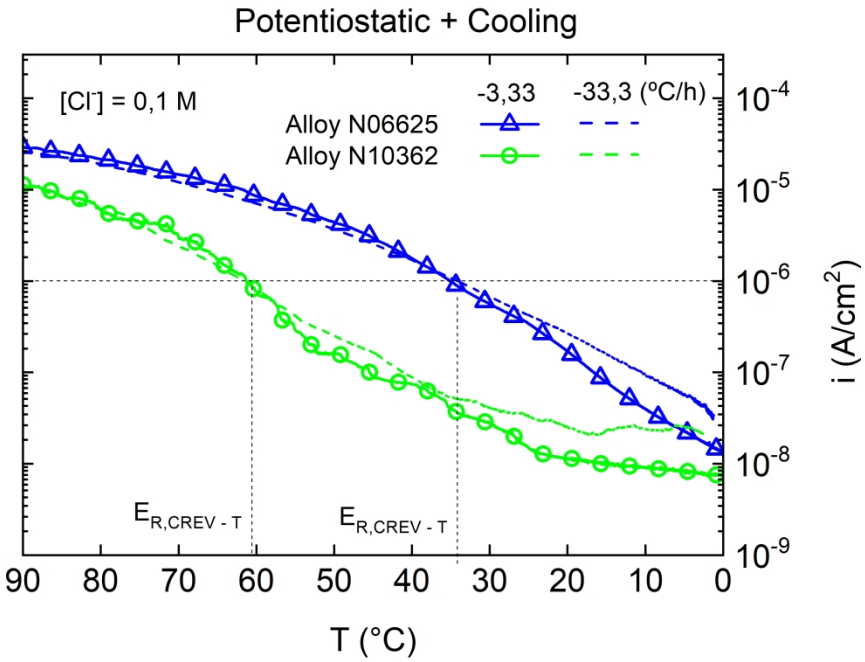
Potentiostatic + Cooling
[Cl⁻] = 0,1 M
-3,33
-33,3 (ºC/h)
Alloy N06625
Alloy N10362
E R,CREV - T
E R,CREV - T
90
80
70
60
50
40
30
20
10
0
T (°C)
10-4
10-5
10-6
10-7
10-8
10-9
i (A/cm2)

Fig 13